

# A Tractable Analysis of the Blind-spot Probability in Localization Networks under Correlated Blocking

Sundar Aditya, *Student Member, IEEE*, Harpreet S. Dhillon, *Member, IEEE*,  
Andreas F. Molisch, *Fellow, IEEE* and Hatim Behairy

## Abstract

In localization applications, the line-of-sight between anchors and targets may be blocked by obstacles in the environment. A target without line-of-sight to enough number of anchors cannot be unambiguously localized and is, therefore, said to be in a *blind-spot*. In this paper, we analyze the blind-spot probability of a typical target by using stochastic geometry to model the randomness in the obstacle and anchor locations. In doing so, we handle correlated anchor blocking induced by obstacles, unlike previous works that assume independent anchor blocking. We first characterize the regime over which the independent blocking assumption underestimates the blind-spot probability of the typical target, which in turn, is characterized as a function of the distribution of the unshadowed area, as seen from the target location. Since this distribution is difficult to characterize exactly, we formulate the *nearest two-obstacle approximation*, which is equivalent to considering correlated blocking for only the nearest two obstacles from the target and assuming independent blocking for the remaining obstacles. Based on this, we derive a closed-form (approximate) expression for the blind-spot probability, which helps determine the anchor deployment intensity needed for the blind-spot probability of a typical target to be at most a threshold,  $\mu$ .

Sundar Aditya and Andreas F. Molisch are with WiDeS, Ming Hsieh Dept. of Electrical Engineering, USC, Los Angeles, CA 90089, USA (Email: {sundarad,molisch}@usc.edu).

Harpreet S. Dhillon is with Wireless@VT, Bradley Dept. of Electrical and Computer Engineering, Virginia Tech, Blacksburg, VA 24061, USA (Email: hdhillon@vt.edu).

Hatim Behairy is with King Abdulaziz City for Science and Technology, P. O. Box 6086, Riyadh 11442, Saudi Arabia (Email: hbehairy@kacst.edu.sa)

Revised: December 3, 2024.

This work was supported by KACST under grant number 33-878. This paper was presented in part at the International Conference on Ubiquitous Wireless Broadband (ICUWB), 2016 held at Nanjing, China [1].

## Index Terms

Localization; line-of-sight (LoS); blind-spot probability; correlated blocking; stochastic geometry; Boolean model; germ-grain model; Poisson point process

## I. INTRODUCTION

Accurate localization is becoming an increasingly indispensable tool for supporting a variety of indoor and outdoor applications such as location-based advertising [2], search-and-rescue operations [3], self-driving vehicles [4], assisted living [5], remote RFID [6]–[8] etc. Many of the above applications require centimeter-level accuracy in environments where the Global Positioning System (GPS) is traditionally unreliable (e.g., indoors, street canyons etc.). A feasible solution to overcome this challenge is to realize a terrestrial wireless localization network by deploying transceivers, known as anchors, throughout the region of interest. For reasons of cost and energy efficiency, each anchor may be equipped with only a single antenna in some deployments. As a result, directional information such as the angle of arrival/departure cannot be exploited from the signal emanating from a target (e.g., a car or an RFID tag). However, when the available bandwidth is large (e.g., millimeter-wave (mmWave) or ultrawideband (UWB) systems), time-of-arrival (ToA) based localization is well suited and can provide accuracies in the sub-centimeter range [9]. In such cases, line-of-sight (LoS) from a target to at least three anchors is required for unambiguous ToA-based localization over a 2D plane<sup>1</sup>.

In many of the applications listed above, the LoS path between two points may be blocked by obstacles such as furniture, walls etc. Since such obstacles are typically not point objects, the blocking of LoS between two or more anchors and a particular target exhibits correlation, in general (e.g., anchors A1 and A2 are blocked to the target by the same obstacle in Fig. 1). A target is said to be in a blind-spot if it has LoS to fewer than three anchors. Ignoring the correlation in LoS blocking events and assuming independent blocking across links instead can result in the underestimation of the blind-spot probability of a given target. For instance, if two anchors, situated close to one another, are each blocked from a target with probability  $p$ , then the joint blocking probability for the anchors is also approximately  $p$ , which exceeds  $p^2$ , the result obtained by assuming independent blocking. This motivates the analysis of the blind-spot

<sup>1</sup>Throughout this work, we assume 2D localization for convenience. The extension to the 3D case is straightforward. In particular, LoS to at least *four* anchors is required for unambiguous 3D localization.

probability of a typical target over a localization network, which is the focus of this work. Our approach is as follows: we assume that the map of the environment is unknown and therefore, treat the obstacle locations and shapes as a realization of a spatial random process (specifically, a Boolean model). Similarly, the anchor locations are drawn from a realization of a homogeneous Poisson point process (PPP). In such a setting, the blind-spot probability at a given location depends on the area of the unshadowed region, as seen from that point. Hence, we characterize the blind-spot probability as a function of the distribution of the unshadowed area.

Although a deterministic, blind-spot eliminating anchor placement can be obtained by solving a variant of the art-gallery problem [10], [11] when the map of the environment is known, there are a number of advantages to using a stochastic geometry based formulation for modeling the obstacles as well as the anchor locations:

- In some environments (e.g., within a home), the positions of obstacles like furniture can change over time. Hence, a new solution for the anchor locations may need to be computed whenever the map of the environment changes, which is especially cumbersome if more anchors are needed to eliminate blind-spots in the altered environment. However, such variations in the environment are inherently captured in our stochastic geometry framework, which provides a trade-off where the elimination of blind-spots is replaced by a probabilistic guarantee as a function of obstacle and anchor statistics instead.
- The number of points in a 2D region for a homogeneous PPP depends only on its area and is agnostic of its shape. This leads to a simpler implementation where the total square footage of the environment, which is much easier to obtain than the detailed floor plan, is sufficient to determine the anchor locations that achieve the desired (probabilistic) performance guarantee (e.g., at most 5% blind-spot probability).
- Finally, in some deployment scenarios (e.g., dropping localization nodes from the air), deterministic placement of anchor nodes is inherently impossible.

In summary, a stochastic geometry analysis characterizes network performance over an ensemble of environment realizations instead of a particular snapshot. In doing so, it provides useful design insights, such as the intensity with which anchors need to be deployed so that the blind-spot probability over the entire region is less than a threshold  $\mu$ .

### A. Related Work

The PPP was used to model base station locations while investigating the *hearability* problem for localization in cellular networks [12], [13], where the hearability metric was defined as the number of base stations whose SINR (signal-to-interference-plus-noise ratio) at a target mobile station crossed a particular threshold. However, independent log-normal shadowing was assumed for all links and the blocked LoS scenario was not specifically addressed. The Boolean model has been used to analyze the impact of blocking on the performance of urban cellular networks [14], and mm-wave systems [15]–[18]. In [14], [16], [17], independent blocking was assumed across different links, while in [18], the spatio-temporal correlation between the LoS/NLoS states of two links was investigated. The effect of correlated shadowing on the interference distribution of wireless networks in urban areas was studied in [19], using a Manhattan line process to model building locations. In the conference version of this paper [1], we partially considered the impact of correlated blocking by estimating the blind-spot probability of a localization network using approximate second-order blocking statistics and in [20], the worst-case impact of correlated blocking on the blind-spot probability was investigated by considering *infinitely* large obstacles modeled by a line process. In general though, to the best of our knowledge, stochastic geometry models for correlated shadowing or blocking in wireless networks remain a scarcely investigated field.

### B. Contributions

The main contributions of this work are as follows:

- We model the anchor locations using a homogeneous PPP and the obstacle locations and shapes using a Boolean model. With respect to a fixed target, the obstacles induce shadow regions that, strictly speaking, do not form a Boolean model [21, Chap. 3], as the area of the shadowed region depends on the proximity of the obstacle to the target. Under these conditions, we express the blind-spot probability as a function of the probability distribution of the unshadowed area.
- We then show that the blind-spot probability under the independent anchor blocking assumption depends only on the mean unshadowed area, instead of the entire probability distribution. In addition, we derive the conditions under which the independent blocking assumption underestimates the true blind-spot probability.

- We then demonstrate that the probability distribution of the unshadowed area is difficult to characterize in closed-form. As a result, we propose an approximate solution for characterizing the unshadowed area whereby in each environment realization, the unshadowed area is evaluated *exactly* up to the location of the second nearest obstacle and the remaining value beyond that is approximated by its mean. We refer to this as the *nearest two-obstacle approximation* and we show that it is equivalent to considering correlated blocking up to the location of the second nearest obstacle and assuming independent blocking for farther obstacles, where the impact of blocking correlation is relatively minimal. In other words, the nearest two-obstacle approximation engenders a *quasi-independent* blocking assumption.
- Using the nearest two-obstacle approximation, we derive a closed-form approximation for the blind-spot probability as well as the conditions under which it yields a tighter bound on the true blind-spot probability, relative to the independent blocking assumption. As a result, our work provides useful design insights, such as the intensity with which anchors need to be deployed so that the blind-spot probability over the entire region is less than a threshold,  $\mu$ .

### C. Notation

Throughout this work, bold lowercase Latin (e.g.,  $\mathbf{a}$ ) or Greek letters (e.g.,  $\alpha$ ) are used to represent vectors.  $\mathbb{R}$  denotes the set of real numbers and  $\nu_2(\cdot)$  denotes the Lebesgue measure in  $\mathbb{R}^2$  (i.e., for a set  $\mathcal{S} \subseteq \mathbb{R}^2$ ,  $\nu_2(\mathcal{S})$  denotes the area of  $\mathcal{S}$ ). The probability of an event  $A$  is denoted by  $\mathbb{P}(A)$  and the expectation operator is denoted either by  $\mathbb{E}_X[\cdot]$ , to explicitly indicate expectation with respect to a random variable,  $X$ ; or by  $\mathbb{E}[\cdot]$ , when the context is clear.  $\bigcup$  and  $\bigcap$  denote set union and intersection, respectively, and  $\emptyset$  denotes the empty set. A real function  $f$ , with argument  $t$  and parameters given by a vector,  $\mathbf{a}$ , is denoted by  $f(t; \mathbf{a})$ . Finally, for a function  $f : \mathbb{R} \rightarrow \mathbb{R}$ ,  $\text{graph}(f) \triangleq \{(x, y) \in \mathbb{R}^2 : y = f(x)\}$  and  $\text{epi}(f) \triangleq \{(x, y) \in \mathbb{R}^2 : y \geq f(x)\}$  denote its graph and epigraph, respectively [22].

### D. Organization

This paper is divided into seven sections. The system model is described in Section II, where the anchor locations are modeled using a homogeneous PPP and the obstacles are represented using line-segments of random lengths and orientations. In Section III, the blind-spot probability

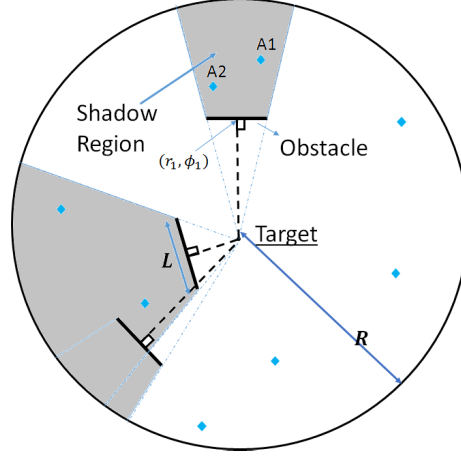


Fig. 1: A localization network consisting of anchors (◆) and obstacles (／) surrounding a target. The distributed obstacles give rise to correlated blocking. The shadow regions can be viewed as a germ-grain model, where the germs are the obstacle mid-points and the grains are the shaded regions.

is characterized as function of the distribution of the unshadowed area. Additionally, the blind-spot probability under the independent anchor blocking assumption is also characterized and the conditions under which it underestimates the true blind-spot probability are derived. The nearest two-obstacle approximation is introduced in Section IV to characterize the unshadowed area in a tractable manner, which is then used to derive an approximate expression for the blind-spot probability in Section V, that takes into account the impact of correlated blocking up to the second nearest obstacle. Numerical results to validate our approximations are presented in Section VI. Finally, Section VII concludes the paper.

## II. SYSTEM MODEL

Consider an environment consisting of point targets and distributed obstacles situated in  $\mathbb{R}^2$ . Intuitively, the  $i$ -th obstacle can be parametrized by the tuple  $(\mathbf{p}_i, \mathcal{S}_i, \omega_i)$ , where  $\mathcal{S}_i \subseteq \mathbb{R}^2$  denotes the ‘shape’ of the obstacle (e.g., a rectangle),  $\mathbf{p}_i = (r_i, \phi_i) \in \mathbb{R}^2$  its ‘location’ in polar coordinates ( $\phi_i \in [0, 2\pi)$ ) (e.g., the geometrical center of the rectangle), and  $\omega_i \in [0, 2\pi)$  its ‘orientation’ with respect to the positive  $x$ -axis. The collection of obstacles,  $\bigcup_i (\mathbf{p}_i, \mathcal{S}_i, \omega_i)$ , forms a germ-grain model if the following conditions are satisfied [23]:

- (i) The set of points  $\{\mathbf{p}_i\}$ , known as germs, form a point process in  $\mathbb{R}^2$ .
- (ii) The set  $\{(\mathcal{S}_i, \omega_i)\}$ , known as grains are drawn from a family of closed sets  $\mathbb{S} \times \Omega$ .

The obstacles are assumed to be opaque to radio waves; hence, it is reasonable to let  $\mathbb{S}$  be the set of line-segments of length at most  $L$ , where  $L$  is the maximum obstacle length (i.e.,  $\mathbb{S} \triangleq [0, L]$ ). Without loss of generality, the germs can be chosen to be the mid-points of the line-segments<sup>2</sup>. Thus,  $\Omega \triangleq [0, \pi)$  is sufficient to encompass all obstacle orientations. We assume the germs to be distributed according to a homogeneous PPP with intensity  $\lambda_0$ . The obstacle lengths and orientations are modeled as samples drawn from a joint distribution, supported on  $\mathbb{S} \times \Omega$ , whose probability density function (pdf) is denoted by  $f_{L,W}(\cdot, \cdot)$ , where  $L$  and  $W$  denote the random variables representing the obstacle length and orientation, respectively.

A localization network comprising of single-antenna anchors is deployed over  $\mathbb{R}^2$  and we assume the anchor locations to also form a homogeneous PPP, with intensity  $\lambda$ , independent of the obstacle germ process. Due to the stationarity of the PPP, it can be assumed without loss of generality that a target is situated at the origin,  $\mathbf{o}$ , which we refer to as the *typical* target. A transmit power constraint further restricts our attention to a disc of radius  $R$ , centered around  $\mathbf{o}$  and denoted by  $\mathcal{D}_{\mathbf{o}}(R)$ , in which anchors must lie for the typical target to be localized. As seen from  $\mathbf{o}$ , the shadow regions induced by the obstacles form a germ-grain model (Fig. 1), where the area of a grain depends on how far its germ (i.e., the corresponding obstacle mid-point) is from  $\mathbf{o}$ . The blocked anchors are those that lie in the shadow region of an obstacle. Since  $f_{L,W}(\cdot, \cdot)$  is usually unknown, we assume all obstacle lengths are equal to  $L$  and  $\omega_i = \phi_i + \pi/2$  (see Fig. 1). If  $r_i \leq R$  (e.g., obstacle with mid-point  $\mathbf{p}_1$  in Fig. 2), then such a rotation of the  $i$ -th obstacle to *face* the (typical) target maximizes the shadow region induced by it; on the other hand, if  $r_i > R$  (e.g., obstacle with mid-point  $\mathbf{p}_2$  in Fig. 2), this rotation eliminates any shadow region otherwise induced by the  $i$ -th obstacle, thereby ignoring the blocking caused by it. As a result, this assumption corresponds to a *quasi worst-case* orientation for the obstacles that emphasizes the (greater) influence of nearer obstacles on correlated anchor blocking and subsequently, the blind-spot probability. In this setting, the typical target can be localized by triangulation if it has LoS to at least three anchors in  $\mathcal{D}_{\mathbf{o}}(R)$ . Consequently, the typical target is said to be in a *blind-spot* if this condition is not satisfied. As blind-spots are undesirable, the blind-spot probability of the typical target is an important metric from a network design perspective. In the following section, we develop the relationship between the blind-spot probability of the typical target and unshadowed area distribution as seen from  $\mathbf{o}$ , which is a function of the obstacle intensity ( $\lambda_0$ )

<sup>2</sup>In general, the germs need not be the geometrical centers of their corresponding grains.

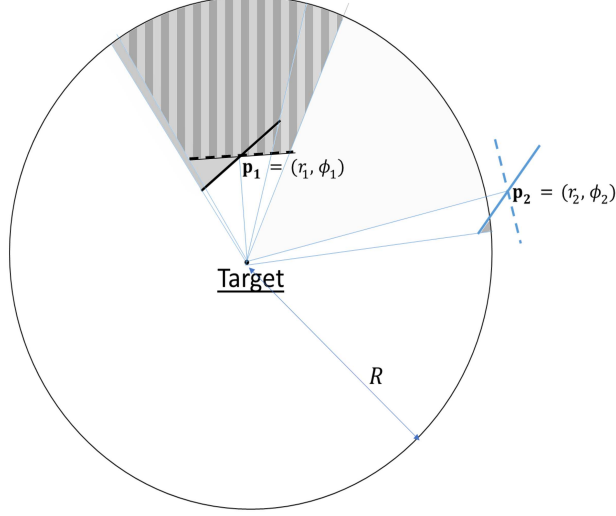


Fig. 2: Illustration of the quasi worst-case obstacle orientation, where all obstacles are assumed to *face* the typical target (illustrated using dotted lines) and have maximum length,  $L$ . This maximizes the shadowed area due to obstacles whose mid-points are within  $\mathcal{D}_o(R)$  (e.g.,  $\mathbf{p}_1$  above). The shadow regions due to the original and ‘rotated’ orientations are represented using the plain and striped grey regions, respectively.), while neglecting the shadowed region induced by obstacles whose mid-points lie outside  $\mathcal{D}_o(R)$  (e.g.,  $\mathbf{p}_2$  above).

and size ( $L$ ).

### III. ANALYSIS OF BLIND-SPOT PROBABILITY

For the parameter vector  $\mathbf{z} = [\lambda_0 \ L \ R]$ , we define the *visibility* random variable, denoted by  $V(\mathbf{p}; \mathbf{z})$  for  $\mathbf{p} = (r, \phi) \in \mathcal{D}_o(R)$ , in the following manner:

$$V(\mathbf{p}; \mathbf{z}) = \begin{cases} 1, & \text{if } \mathbf{p} \text{ is not blocked to } \mathbf{o} \\ 0, & \text{else.} \end{cases} \quad (1)$$

Let  $\mathcal{V}(\mathbf{z}) = \{\mathbf{p} \in \mathcal{D}_o(R) : V(\mathbf{p}; \mathbf{z}) = 1\}$  denote the (random) set of points that have LoS to the typical target and let  $A_v(\mathbf{z}) = \nu_2(\mathcal{V}(\mathbf{z}))$  denote the area of the unshadowed region in  $\mathcal{D}_o(R)$ , as seen from the typical target’s perspective. The typical target is in a blind-spot if and only if there are fewer than three anchors in  $\mathcal{V}(\mathbf{z})$ . Thus, the blind-spot probability, conditioned on the random variable  $A_v(\mathbf{z})$  and denoted by  $g(A_v(\mathbf{z}); \lambda)$ , with parameter  $\lambda$ , has the following expression:

$$g(A_v(\mathbf{z}); \lambda) \triangleq \mathbb{P}(\text{blind-spot} \mid A_v(\mathbf{z}))$$



$$= \sum_{k=0}^2 \mathbb{P}(k \text{ anchors present in the unshadowed region of area } A_v(\mathbf{z})) \quad (2)$$

$$= e^{-\lambda A_v(\mathbf{z})} \left( 1 + \lambda A_v(\mathbf{z}) + \frac{(\lambda A_v(\mathbf{z}))^2}{2} \right). \quad (3)$$

The unconditional blind-spot probability,  $b(\lambda, \mathbf{z})$ , is then obtained by averaging over the distribution of  $A_v(\mathbf{z})$  as given below,

$$b(\lambda, \mathbf{z}) = \int_0^{\pi R^2} g(t; \lambda) f_{A_v(\mathbf{z})}(t) dt, \quad (4)$$

where  $f_{A_v(\mathbf{z})}(\cdot)$  is the pdf of  $A_v(\mathbf{z})$ , which fully captures the statistics of correlated anchor blocking due to obstacle size  $L$  and intensity  $\lambda_0$ .

On the other hand, if we ignore the blocking correlation and assume independent anchor blocking instead, the resulting blind-spot probability is given by the following lemma:

**Lemma 1.** *The blind-spot probability under the independent anchor blocking assumption, denoted by  $b^{\text{ind}}(\lambda, \mathbf{z})$ , is given by:*

$$b^{\text{ind}}(\lambda, \mathbf{z}) = e^{-\lambda \mathbb{E}[A_v(\mathbf{z})]} \left( 1 + \lambda \mathbb{E}[A_v(\mathbf{z})] + \frac{(\lambda \mathbb{E}[A_v(\mathbf{z})])^2}{2} \right) = g(\mathbb{E}[A_v(\mathbf{z})]; \lambda). \quad (5)$$

*Proof:* See Appendix A. ■

**Corollary 1.**  *$f_{A_v(\mathbf{z})}(t) = \delta(t - \mathbb{E}[A_v])$  for independent anchor blocking, where  $\delta(\cdot)$  denotes the Dirac-delta function.*

*Proof:* See Appendix B. ■

From Lemma 1, it can be seen that the mean unshadowed area,  $\mathbb{E}[A_v(\mathbf{z})]$ , completely characterizes the blind-spot probability if independent anchor blocking is assumed. For the system model from Section II,  $\mathbb{E}[A_v(\mathbf{z})]$  is given by the following lemma:

**Lemma 2.** *For a parameter vector  $\mathbf{z}$ , the average unshadowed area,  $\mathbb{E}[A_v(\mathbf{z})]$ , over  $\mathcal{D}_o(R)$  is given by:*

$$\mathbb{E}[A_v(\mathbf{z})] = 2\pi \int_0^R \exp(-\lambda_0 \nu_2(\mathcal{S}_V(\mathbf{p}; \mathbf{z}))) r dr d\phi, \quad (6)$$

$$\text{where } \mathcal{S}_V(\mathbf{p}; \mathbf{z}) = \{(\rho, \beta) \in \mathbb{R}^2 : 0 \leq \rho \tan |\beta - \phi| \leq L/2, 0 \leq \rho \sec |\beta - \phi| \leq r\} \quad (7)$$

$$\text{and } \nu_2(\mathcal{S}_V(\mathbf{p}; \mathbf{z})) = 2 \int_0^r \rho \min \left( \arctan \left( \frac{L}{2\rho} \right), \arccos \left( \frac{\rho}{r} \right) \right) d\rho. \quad (8)$$

*Proof:* See Appendix C. ■

The relationship between  $b(\lambda, \mathbf{z})$  and  $b^{\text{ind}}(\lambda, \mathbf{z})$  is given by the following theorem:

**Theorem 1.**  $b^{\text{ind}}(\lambda, \mathbf{z}) \leq b(\lambda, \mathbf{z})$  over  $\{(\lambda, \mathbf{z}) : \lambda \mathbb{E}[A_v(\mathbf{z})] \geq 3.3836\}$ .

*Proof:* As a twice-differentiable function of  $t$ , we have

$$\frac{d}{dt}g(t; \lambda) = -(\lambda^3/2)t^2e^{-\lambda t} \quad (9)$$

$$\frac{d^2}{d^2t}g(t; \lambda) = (\lambda^3/2)te^{-\lambda t}(\lambda t - 2). \quad (10)$$

From (10), the second derivative of  $g(t; \lambda)$  is non-negative when  $t \geq 2/\lambda$ . Hence,  $g(t; \lambda)$  is a convex function in  $t$  over this regime [22]. Let  $t_0$  denote the solution to the following equation:

$$1 = g(0; \lambda) = g(t_0; \lambda) - t_0 \frac{d}{dt}g(t; \lambda) \Big|_{t=t_0} \quad (11)$$

$$\implies 1 = e^{-\lambda t_0} \left[ \frac{(\lambda t_0)^3}{2} + \frac{(\lambda t_0)^2}{2} + \lambda t_0 + 1 \right]. \quad (12)$$

Eqn. (12) is a mixed polynomial-exponential equation in  $\lambda t_0$  and solving for  $\lambda t_0$  numerically, we obtain (up to four digits of precision),

$$t_0 = \frac{3.3836}{\lambda}. \quad (13)$$

Geometrically,  $t_0$  determines the  $x$ -coordinate of the point at which the line  $y(t; \lambda) \subseteq \mathbb{R}^2$ , passing through  $(0, g(0; \lambda))$ , is tangential to  $\text{epi}(g(\cdot; \lambda))$ , as shown in Fig. 3. The equation of  $y(t; \lambda)$  is as follows:

$$y(t; \lambda) = g(t_0; \lambda) + (t - t_0) \frac{d}{dt}g(t; \lambda) \Big|_{t=t_0}, \quad t \geq 0. \quad (14)$$

Let

$$g_{\text{con}}(t; \lambda) = \begin{cases} g(t; \lambda), & t > t_0 \\ y(t; \lambda), & t \leq t_0. \end{cases} \quad (15)$$

For  $0 \leq t \leq t_0$ , the supporting hyperplane at each point,  $(t, g_{\text{con}}(t; \lambda))$ , on the boundary of  $\text{epi}(g_{\text{con}}(\cdot; \lambda))$  is  $y(\cdot; \lambda)$ . Similarly, there also exists a supporting hyperplane at each boundary point,  $(t, g_{\text{con}}(t; \lambda))$ , of  $\text{epi}(g_{\text{con}}(\cdot; \lambda))$  for  $t > t_0$ , since  $g_{\text{con}}(\cdot; \lambda) \equiv g(\cdot; \lambda)$ , a convex function in its argument over this interval [22]. Thus,  $g_{\text{con}}(t; \lambda)$  is a convex function in  $t$  for  $t \geq 0$ . Consequently, if  $\mathbb{E}[A_v(\mathbf{z})] > t_0$ , then

$$b^{\text{ind}}(\lambda, \mathbf{z}) = g(\mathbb{E}[A_v(\mathbf{z})]; \lambda) \stackrel{a}{=} g_{\text{con}}(\mathbb{E}[A_v(\mathbf{z})]; \lambda) \stackrel{b}{\leq} \mathbb{E}[g_{\text{con}}(A_v(\mathbf{z}); \lambda)] \stackrel{c}{\leq} \mathbb{E}[g(A_v(\mathbf{z}); \lambda)] \stackrel{d}{=} b(\lambda, \mathbf{z}), \quad (16)$$

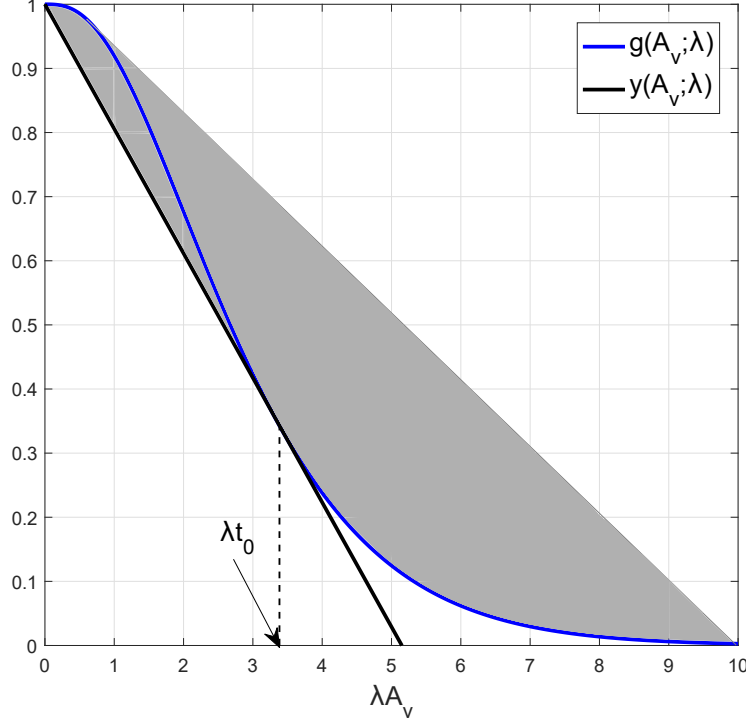


Fig. 3: For  $\lambda \mathbb{E}[A_v(\mathbf{z})] \geq \lambda t_0 = 3.3836$ , the set of points  $\{(\mathbb{E}[A_v(\mathbf{z})], b(\lambda, \mathbf{z}))\}$  (i.e., the grey shaded region) lies above the set  $\{(\mathbb{E}[A_v(\mathbf{z})], b^{\text{ind}}(\lambda, \mathbf{z}))\}$ , shown by the blue curve.

where (a) follows from (15), (b) from Jensen's inequality, (c) from the fact that  $g_{\text{con}}(t; \lambda) \leq g(t; \lambda)$  for all  $t \geq 0$ , and (d) from the definition of  $b(\lambda, \mathbf{z})$  in (4). ■

**Remark 1.** A geometric interpretation of Theorem 1 is seen in Fig. 3, where, as a result of (d) in 16, the feasible values for the ordered pair  $(\mathbb{E}[A_v(\mathbf{z})], b(\lambda, \mathbf{z}))$  is given by the convex hull of  $\text{graph}(g(\cdot; \lambda))$ . On the other hand, the feasible values for  $(\mathbb{E}[A_v(\mathbf{z})], b^{\text{ind}}(\lambda, \mathbf{z}))$  is  $\text{graph}(g(\cdot; \lambda))$ , which forms the lower boundary of its convex hull when  $\lambda \mathbb{E}[A_v(\mathbf{z})] \geq \lambda t_0 = 3.3836$ . It is important to note that Theorem 1 is a consequence of the convexity properties of  $g(\cdot; \lambda)$  and, in particular, does not depend on  $f_{A_v(\mathbf{z})}(\cdot)$ . Thus, the inequality  $b^{\text{ind}}(\lambda, \mathbf{z}) \leq b(\lambda, \mathbf{z})$  may still hold over a set  $\mathcal{Z} \supseteq \{(\lambda, \mathbf{z}) : \lambda \mathbb{E}[A_v(\mathbf{z})] \geq 3.3836\}$  for some choice(s) of  $f_{A_v(\mathbf{z})}(\cdot)$ .

From a design perspective, it is desirable to have at least three unblocked anchors, on average (i.e.,  $\lambda \mathbb{E}[A_v(\mathbf{z})] \geq 3$ ). Hence, from Theorem 1, it is clear that the independent blocking assumption underestimates the true blind-spot probability for most practical scenarios and that correlated blocking should be taken into account while designing a localization network that

meets a desired blind-spot probability threshold. From (2)-(4), it is evident that the distribution of the unshadowed area plays a critical role in determining the blind-spot probability of the typical target, for a given anchor intensity  $\lambda$ . In the next section, we attempt to characterize this distribution.

#### IV. CHARACTERIZING UNSHADOWED AREA

The area of the unshadowed region surrounding the typical target depends on the number of obstacles as well as their locations. To capture this dependence, we define the following:

**Definition 1.** Let  $\mathcal{V}(\mathbf{p}^{(k)}; \mathbf{z})$  denote a realization of  $\mathcal{V}(\mathbf{z})$  when  $k(> 0)$  obstacle(s) are present, with the obstacle locations determined by  $\mathbf{p}^{(k)} = [\mathbf{r}^{(k)} \ \boldsymbol{\phi}^{(k)}]$ , where  $\mathbf{r}^{(k)} = [r_1 \ \cdots \ r_k]$  ( $r_i \leq r_j, i < j$ ),  $\boldsymbol{\phi}^{(k)} = [\phi_1 \ \cdots \ \phi_k]$ , and the  $i$ -th nearest obstacle mid-point is located at  $(r_i, \phi_i)$ , ( $i = 1, \dots, k$ ). The special case when  $k = 0$  is denoted by  $\mathcal{V}(\emptyset; \mathbf{z})$  and is equal to  $\mathcal{D}_o(R)$ .

**Definition 2.** Let  $A_v^{(k)}(\mathbf{p}^{(k)}; \mathbf{z})$  denote the area of the unshadowed region given by  $\mathcal{V}(\mathbf{p}^{(k)}; \mathbf{z})$  (i.e.,  $A_v^{(k)}(\mathbf{p}^{(k)}; \mathbf{z}) \triangleq \nu_2(\mathcal{V}(\mathbf{p}^{(k)}; \mathbf{z}))$ ). In particular,  $A_v^{(k)}(\mathbf{p}^{(k)}; \mathbf{z})$  is a realization of the random variable  $A_v(\mathbf{z})$ , conditioned on the presence of  $k$  obstacles whose locations are given by  $\mathbf{p}^{(k)}$ .

For  $k < 2$ ,  $A_v^{(k)}(\mathbf{p}^{(k)}; \mathbf{z})$  is easy to characterize,

$$A_v^{(0)}(\emptyset; \mathbf{z}) = \pi R^2 \quad (17)$$

$$A_v^{(1)}(\mathbf{p}_1; \mathbf{z}) = \pi R^2 - \underbrace{\left( \frac{\theta(\mathbf{p}_1; \mathbf{z})}{2} R^2 - \frac{1}{2} r_1 x(\mathbf{p}_1; \mathbf{z}) \right)}_{\text{Shadowed area}}, \quad (18)$$

$$\text{where } \theta(\mathbf{p}_1; \mathbf{z}) = \begin{cases} 2 \arctan \left( \frac{L}{2r_1} \right) , & 0 \leq r_1 \leq \sqrt{R^2 - (L/2)^2} \\ 2 \arccos \left( \frac{r_1}{R} \right) , & \sqrt{R^2 - (L/2)^2} \leq r_1 \leq R \end{cases} \quad (19)$$

$$x(\mathbf{p}_1; \mathbf{z}) = \begin{cases} L , & 0 \leq r_1 \leq \sqrt{R^2 - (L/2)^2} \\ 2\sqrt{R^2 - r_1^2} , & \sqrt{R^2 - (L/2)^2} \leq r_1 \leq R. \end{cases} \quad (20)$$

In particular, the term in parenthesis in (18) denotes the shadowed area (Fig. 4).

For  $k \geq 2$ , overlaps may occur between the shadow regions corresponding to different obstacles (see Fig. 1). In order to accurately determine  $A_v^{(k)}(\mathbf{p}^{(k)}; \mathbf{z})$ , the areas of all overlapping shadowed regions should be counted exactly once. We first attempt to characterize the shadow region overlap corresponding to the nearest two obstacles, for which we define the following:

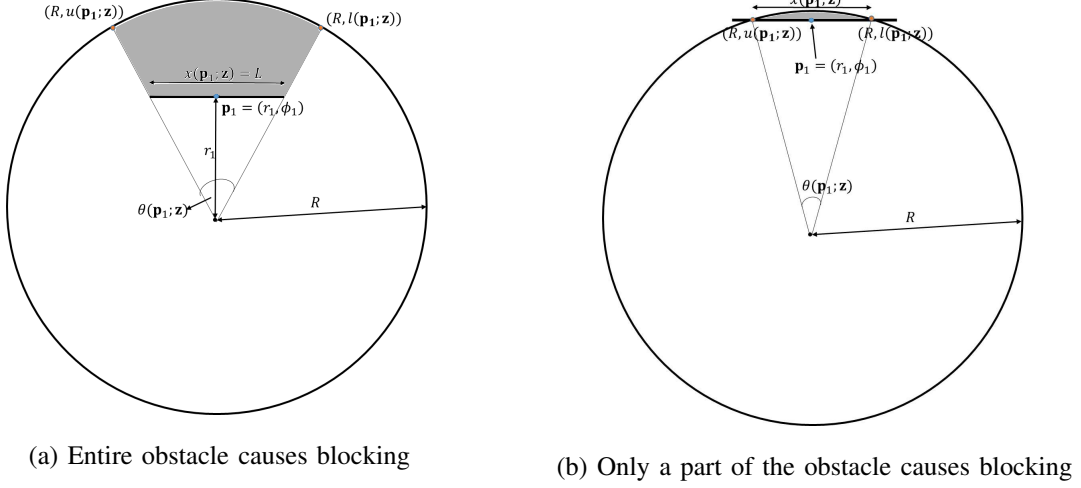


Fig. 4: Shadowed area (shaded gray) due to a single obstacle.

**Definition 3.** Let  $\mathcal{A}_{\text{sh}}(\mathbf{p}; \mathbf{z}) \subseteq \mathcal{D}_o(R)$  denote the shadow region induced by an obstacle whose mid-point is at  $\mathbf{p}$  (e.g., Fig. 4). The azimuthal end-points of  $\mathcal{A}_{\text{sh}}(\mathbf{p}; \mathbf{z})$ , denoted by  $l(\mathbf{p}; \mathbf{z})$  and  $u(\mathbf{p}; \mathbf{z})$ , are given by the following expressions:

$$l(\mathbf{p}; \mathbf{z}) = \left( \phi - \frac{\theta(\mathbf{p}; \mathbf{z})}{2} \right) \mod 2\pi \quad (21)$$

$$u(\mathbf{p}; \mathbf{z}) = \left( \phi + \frac{\theta(\mathbf{p}; \mathbf{z})}{2} \right) \mod 2\pi, \quad (22)$$

where  $\theta(\mathbf{p}; \mathbf{z})$  is given by (19). Thus, the azimuthal span of  $\mathcal{A}_{\text{sh}}(\mathbf{p}; \mathbf{z})$ , denoted by the interval  $\mathcal{I}(\mathbf{p}; \mathbf{z}) \subseteq [0, 2\pi)$ , has the following expression:

$$\mathcal{I}(\mathbf{p}; \mathbf{z}) = [\min(l(\mathbf{p}; \mathbf{z}), u(\mathbf{p}; \mathbf{z})), \max(l(\mathbf{p}; \mathbf{z}), u(\mathbf{p}; \mathbf{z}))]. \quad (23)$$

A typical overlap between a pair of shadow regions  $\mathcal{A}_{\text{sh}}(\mathbf{p}_1; \mathbf{z})$  and  $\mathcal{A}_{\text{sh}}(\mathbf{p}_2; \mathbf{z})$  is illustrated in Fig. 5 and the extent of overlap can be characterized by the following lemma.

**Lemma 3.** Let  $\alpha(\mathbf{p}^{(2)}; \mathbf{z}) \in [0, 1]$  denote the fraction of  $\mathcal{A}_{\text{sh}}(\mathbf{p}_2; \mathbf{z})$  that overlaps with  $\mathcal{A}_{\text{sh}}(\mathbf{p}_1; \mathbf{z})$  in the azimuth. Then,

$$\alpha(\mathbf{p}^{(2)}; \mathbf{z}) = \max \left( 0, \frac{\epsilon(\mathbf{p}^{(2)}; \mathbf{z})}{\theta(\mathbf{p}_2; \mathbf{z})} \right), \quad (24)$$

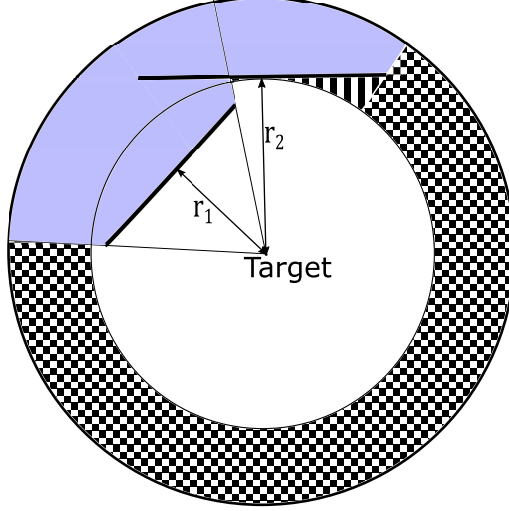


Fig. 5: The shaded region denotes the area shadowed by the nearest two obstacles. The additional shadow region induced by the third nearest obstacle onwards must intersect the part-annular checkered region.

$$\text{where } \epsilon(\mathbf{p}^{(2)}; \mathbf{z}) = \begin{cases} \min(u(\mathbf{p}_1; \mathbf{z}), u(\mathbf{p}_2; \mathbf{z})) - \max(l(\mathbf{p}_1; \mathbf{z}), l(\mathbf{p}_2; \mathbf{z})), & \text{if} \\ \quad l(\mathbf{p}_1; \mathbf{z}) \leq u(\mathbf{p}_1; \mathbf{z}), l(\mathbf{p}_2; \mathbf{z}) \leq u(\mathbf{p}_2; \mathbf{z}) \\ 2\pi - (\max(l(\mathbf{p}_1; \mathbf{z}), l(\mathbf{p}_2; \mathbf{z})) - \min(u(\mathbf{p}_1; \mathbf{z}), u(\mathbf{p}_2; \mathbf{z}))), & \text{if} \\ \quad l(\mathbf{p}_1; \mathbf{z}) > u(\mathbf{p}_1; \mathbf{z}), l(\mathbf{p}_2; \mathbf{z}) > u(\mathbf{p}_2; \mathbf{z}) \\ \max(u(\mathbf{p}_2; \mathbf{z}) - l(\mathbf{p}_1; \mathbf{z}), u(\mathbf{p}_1; \mathbf{z}) - l(\mathbf{p}_2; \mathbf{z})), & \text{else.} \end{cases} \quad (25)$$

*Proof:* See Appendix D ■

The unshadowed region beyond a radius  $r_2$  can be decomposed into the union of two sets,  $\mathcal{V}_{\text{in}}(\mathbf{p}^{(k)}; \mathbf{z})$  and  $\mathcal{V}_{\text{out}}(\mathbf{p}^{(k)}; \mathbf{z})$ , which are defined as follows:

$$\mathcal{V}_{\text{in}}(\mathbf{p}^{(k)}; \mathbf{z}) = \{\mathbf{p} \in \mathcal{V}(\mathbf{z}) : r > r_2, \phi \in \mathcal{I}(\mathbf{p}_1; \mathbf{z}) \cup \mathcal{I}(\mathbf{p}_2; \mathbf{z})\} \quad (26)$$

$$\mathcal{V}_{\text{out}}(\mathbf{p}^{(k)}; \mathbf{z}) = \{\mathbf{p} \in \mathcal{V}(\mathbf{z}) : r > r_2, \phi \notin \mathcal{I}(\mathbf{p}_1; \mathbf{z}) \cup \mathcal{I}(\mathbf{p}_2; \mathbf{z})\}. \quad (27)$$

$\mathcal{V}_{\text{in}}(\mathbf{p}^{(k)}; \mathbf{z})$  is the (vertically) striped region in Fig. 5 and  $\mathcal{V}_{\text{out}}(\mathbf{p}^{(k)}; \mathbf{z})$  is a subset of the annular region from  $r_2$  to  $R$ , excluding the azimuthal end points of  $\mathcal{A}_{\text{sh}}(\mathbf{p}_1; \mathbf{z}) \cup \mathcal{A}_{\text{sh}}(\mathbf{p}_2; \mathbf{z})$ , i.e., the checkered region in Fig. 5. Using the terminology defined so far,  $A_v^{(k)}(\mathbf{p}^{(k)}; \mathbf{z})$  can be expressed as follows:

$$A_v^{(k)}(\mathbf{p}^{(k)}; \mathbf{z}) = A_{n2}(\mathbf{p}^{(2)}; \mathbf{z}) + A_f(\mathbf{p}^{(k)}; \mathbf{z}), \quad (28)$$

$$\text{where } A_{n2}(\mathbf{p}^{(2)}; \mathbf{z}) \triangleq \pi r_2^2 - \left( \frac{\theta(\mathbf{p}_1; \tilde{\mathbf{z}})}{2} r_2^2 - \frac{1}{2} x(\mathbf{p}_1; \tilde{\mathbf{z}}) r_1 \right) \quad (29)$$

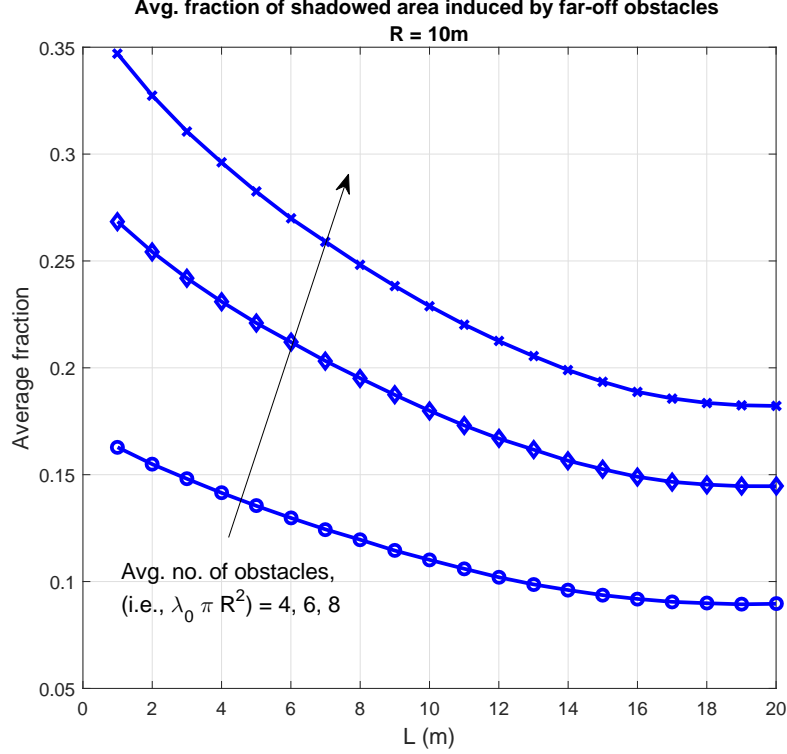


Fig. 6: The nearest two obstacles are responsible for 65 – 90% of the shadowed area. The above curves have been generated by averaging over  $10^6$  Monte-Carlo simulations.

$$\tilde{\mathbf{z}} = [\lambda_0 \ L \ r_2] \quad (30)$$

$$A_f(\mathbf{p}^{(k)}; \mathbf{z}) \triangleq \nu_2(\mathcal{V}_{\text{in}}(\mathbf{p}^{(k)}; \mathbf{z})) + \nu_2(\mathcal{V}_{\text{out}}(\mathbf{p}^{(k)}; \mathbf{z})). \quad (31)$$

In (28)-(31),  $A_{n2}(\mathbf{p}^{(2)}; \mathbf{z})$  denotes the area of the unshadowed region up to the location of the second nearest obstacle (i.e., the area of the white region in Fig. 5) and  $A_f(\mathbf{p}^{(k)}; \mathbf{z})$  denotes the area of the remaining unshadowed region, beyond the second nearest obstacle.

For  $k > 2$ , evaluating the pairwise shadow region overlaps is, in general, insufficient, as more than two obstacles may contribute to a common overlapping region. Since it is not straightforward to ensure that the areas of all overlapping shadowed regions are counted exactly once,  $A_f(\mathbf{p}^{(k)}; \mathbf{z})$  is difficult to compute exactly. Consequently,  $f_{A_v(\mathbf{z})}(\cdot)$  is hard to characterize in closed-form, as well. Hence, we focus on approximating  $A_f(\mathbf{p}^{(k)}; \mathbf{z})$  in the remainder of this section, which shall then be used to derive a tractable approximation for  $b(\lambda, \mathbf{z})$  in the following section.

Since nearer obstacles induce larger shadow regions, it is intuitive that the nearest two obstacles should be responsible for a large fraction of the total shadowed area. To quantify this notion, the fraction of the total shadowed area contributed by the far-off obstacles (i.e., all

obstacles excluding the nearest two obstacles) is plotted in Fig. 6, where it can be seen that the nearest two obstacles account for between 65 – 90%, on average, of the shadowed area. Since the contribution of the far-off obstacles to the total shadowed area is relatively small, it is reasonable to approximate it by its mean value, conditioned on  $\mathbf{p}^{(2)}$ . Thus,  $A_f(\mathbf{p}^{(k)}; \mathbf{z})$  can also be approximated by its mean value, conditioned on  $\mathbf{p}^{(2)}$ . We refer to this as the *nearest two-obstacle approximation*, which is formally expressed below:

**Approximation 1** (Nearest two-obstacle approximation). *For  $k \geq 2$ ,*

$$\begin{aligned} A_v^{(k)}(\mathbf{p}^{(k)}; \mathbf{z}) &\approx A_v^{(2+)}(\mathbf{p}^{(2)}; \mathbf{z}) \\ &\triangleq A_{n2}(\mathbf{p}^{(2)}; \mathbf{z}) + \mathbb{E}[A_f(\mathbf{p}^{(k)}; \mathbf{z}) | \mathbf{p}^{(2)}] \end{aligned} \quad (32)$$

$$\approx A_{n2}(\mathbf{p}^{(2)}; \mathbf{z}) + \mathbb{E}[\nu_2(\mathcal{V}_{\text{out}}(\mathbf{p}^{(k)}; \mathbf{z})) | \mathbf{p}^{(2)}]. \quad (33)$$

In evaluating the conditional mean of  $A_f(\mathbf{p}^{(k)}; \mathbf{z})$  in (32), given  $\mathbf{p}^{(2)}$ , we average over both the *number* and the *locations* of the far-off obstacles, i.e., over both  $k$  and  $\mathbf{p}^{(3:k)}$ , respectively. The approximation in (33) is obtained from (31) by ignoring the term  $\mathbb{E}[\nu_2(\mathcal{V}_{\text{in}}(\mathbf{p}^{(k)}; \mathbf{z})) | \mathbf{p}^{(2)}]$  (i.e., the average area of the striped region in Fig. 5) for the sake of tractability. However, it is easy to observe from Fig. 5 that the area of the striped region increases with increasing obstacle size. As a result, the approximation in (33) may not be reasonable beyond a certain value of  $L$ . In the following lemma, we derive an expression for  $\mathbb{E}[\nu_2(\mathcal{V}_{\text{out}}(\mathbf{p}^{(k)}; \mathbf{z})) | \mathbf{p}^{(2)}]$ .

**Lemma 4.** *Conditioned on the nearest two obstacles, the average unshadowed area over  $\mathcal{V}_{\text{out}}$  is given by*

$$\begin{aligned} \mathbb{E}[\nu_2(\mathcal{V}_{\text{out}}(\mathbf{p}^{(k)}; \mathbf{z})) | \mathbf{p}^{(2)}] &= (2\pi - \theta(\mathbf{p}_1; \mathbf{z}) - (1 - \alpha(\mathbf{p}^{(2)}; \mathbf{z}))\theta(\mathbf{p}_2; \mathbf{z})) \times \\ &\quad \int_{r_2}^R \exp \left( -2\lambda_0 \int_{r_2}^r \rho \min \left( \arctan \left( \frac{L}{2\rho} \right), \arccos \left( \frac{\rho}{r} \right) \right) d\rho \right) dr. \end{aligned} \quad (34)$$

*Proof:* See Appendix E. ■

**Remark 2.** *The nearest two-obstacle approximation characterizes the unshadowed area beyond the second nearest obstacle only by its mean. However, from Lemma 1 and Corollary 1, this is equivalent to assuming independent blocking beyond the second nearest obstacle. Hence, the nearest two-obstacle approximation can also be interpreted as a ‘quasi-independent blocking assumption’.*



In the next section, we derive a tractable approximation for  $b(\lambda, \mathbf{z})$  using the nearest two-obstacle approximation.

## V. A TRACTABLE APPROXIMATION FOR $b(\lambda, \mathbf{z})$

Let  $b_k(\lambda, \mathbf{z})$  denote the blind-spot probability, conditioned on  $k$  obstacles being present, for anchor intensity  $\lambda$  and parameter vector  $\mathbf{z}$ . By first conditioning and then averaging over the obstacle locations,  $b_k(\lambda, \mathbf{z})$  can be expressed as follows:

$$b_k(\lambda, \mathbf{z}) = \int_0^{2\pi} \int_0^R f^{(k)}(\mathbf{p}_1) d\mathbf{p}_1 \cdots \int_0^{2\pi} \int_{r_{k-1}}^R g(A_v^{(k)}(\mathbf{p}^{(k)}; \mathbf{z}); \lambda) f^{(k)}(\mathbf{p}_k | \mathbf{p}^{(k-1)}) d\mathbf{p}_k \quad (35)$$

$$= \int_0^{2\pi} \int_0^R f^{(k)}(\mathbf{p}_1) d\mathbf{p}_1 \cdots \int_0^{2\pi} \int_{r_{k-1}}^R g(A_v^{(k)}(\mathbf{p}^{(k)}; \mathbf{z}); \lambda) f^{(k)}(\mathbf{p}_k | \mathbf{p}_{k-1}) d\mathbf{p}_k, \quad (36)$$

where  $d\mathbf{p}_i = r_i dr_i d\phi_i$  ( $i = 1, \dots, k$ ) and  $f^{(k)}(\mathbf{p}_i | \mathbf{p}^{(i-1)})$  in (35) denotes the conditional pdf of the location of the  $i$ -th ( $2 \leq i \leq k$ ) nearest obstacle given the location(s) of the other obstacles that are closer to the target than it, when a total of  $k$  obstacles are present. Similarly,  $f^{(k)}(\mathbf{p}_1)$  denotes the pdf of the location of the nearest obstacle. The simplification in (36) is a result of the Markov property, since  $r_i$  lies in the interval  $[r_{i-1}, R]$  and is therefore independent of  $r_j$  for  $j \in \{1, \dots, i-2\}$ , given  $r_{i-1}$ .

For  $k < 2$ ,  $b_k(\lambda, \mathbf{z})$  is expressed as follows:

$$b_0(\lambda, \mathbf{z}) = g(A_v^{(0)}(\emptyset; \mathbf{z}); \lambda) \quad (37)$$

$$b_1(\lambda, \mathbf{z}) = \int_0^{2\pi} \int_0^R g(A_v^{(1)}(\mathbf{p}_1; \mathbf{z}); \lambda) \frac{1}{\pi R^2} d\mathbf{p}_1. \quad (38)$$

For  $k \geq 2$ , the nearest two-obstacle approximation is used to simplify  $b_k(\lambda, \mathbf{z})$ , as given below,

$$b_k(\lambda, \mathbf{z}) \approx b_k^{(2+)}(\lambda, \mathbf{z}) \quad (39)$$

$$\triangleq \int_0^{2\pi} \int_0^R f^{(k)}(\mathbf{p}_1) d\mathbf{p}_1 \int_0^{2\pi} \int_{r_1}^R f^{(k)}(\mathbf{p}_2 | \mathbf{p}_1) d\mathbf{p}_2 \cdots \int_0^{2\pi} \int_{r_{k-1}}^R g(A_v^{(2+)}(\mathbf{p}^{(2)}; \mathbf{z}); \lambda) f^{(k)}(\mathbf{p}_k | \mathbf{p}_{k-1}) d\mathbf{p}_k \quad (40)$$

$$= \int_0^{2\pi} \int_0^R f^{(k)}(\mathbf{p}_1) d\mathbf{p}_1 \int_0^{2\pi} \int_{r_1}^R g(A_v^{(2+)}(\mathbf{p}^{(2)}; \mathbf{z}); \lambda) f^{(k)}(\mathbf{p}_2 | \mathbf{p}_1) d\mathbf{p}_2, \quad (41)$$

where  $A_v^{(2+)}(\mathbf{p}^{(2)}; \mathbf{z})$  is given by (33). The expressions for  $f^{(k)}(\mathbf{p}_1)$  and  $f^{(k)}(\mathbf{p}_2|\mathbf{p}_1)$  are as follows:

$$f^{(k)}(\mathbf{p}_1) = \frac{k}{\pi R^2} \left( \frac{R^2 - r_1^2}{R^2} \right)^{k-1} \quad (42)$$

$$f^{(k)}(\mathbf{p}_2|\mathbf{p}_1) = \frac{k-1}{\pi(R^2 - r_1^2)} \left( \frac{R^2 - r_2^2}{R^2 - r_1^2} \right)^{k-2} \quad (43)$$

with (42) and (43) following as a result of the  $k$  obstacle mid-points being independently and uniformly distributed over  $\mathcal{D}_o(R)$ .

Using (37)-(43), an approximate expression for  $b(\lambda, \mathbf{z})$  can be derived by first conditioning and then averaging over the number of obstacles,  $k$ , in the following manner:

$$b(\lambda, \mathbf{z}) = \sum_{k=0}^{\infty} b_k(\lambda, \mathbf{z}) e^{-\lambda_0 \pi R^2} \frac{(\lambda_0 \pi R^2)^k}{k!} \quad (44)$$

$$\approx b_0(\lambda, \mathbf{z}) e^{-\lambda_0 \pi R^2} + b_1(\lambda, \mathbf{z}) e^{-\lambda_0 \pi R^2} (\lambda_0 \pi R^2) + \sum_{k=2}^{\infty} b_k^{(2+)}(\lambda, \mathbf{z}) e^{-\lambda_0 \pi R^2} \frac{(\lambda_0 \pi R^2)^k}{k!} \quad (45)$$

$$\begin{aligned} &= g(A_v^{(0)}(\emptyset; \mathbf{z}); \lambda) e^{-\lambda_0 \pi R^2} + \left( \int_0^{2\pi} \int_0^R g(A_v^{(1)}(\mathbf{p}_1; \mathbf{z}); \lambda) \frac{1}{\pi R^2} r_1 dr_1 d\phi_1 \right) e^{-\lambda_0 \pi R^2} (\lambda_0 \pi R^2) \\ &+ \int_0^{2\pi} \int_0^R d\mathbf{p}_1 \int_0^{2\pi} \int_{r_1}^R g(A_v^{(2+)}(\mathbf{p}^{(2)}; \mathbf{z}); \lambda) e^{-\lambda_0 \pi R^2} \left( \sum_{k=2}^{\infty} f^{(k)}(\mathbf{p}_1) f^{(k)}(\mathbf{p}_2|\mathbf{p}_1) \frac{(\lambda_0 \pi R^2)^k}{k!} \right) d\mathbf{p}_2 \end{aligned} \quad (46)$$

$$\begin{aligned} &= g(A_v^{(0)}(\emptyset; \mathbf{z}); \lambda) e^{-\lambda_0 \pi R^2} + \left( \int_0^{2\pi} \int_0^R g(A_v^{(1)}(\mathbf{p}_1; \mathbf{z}); \lambda) \frac{1}{\pi R^2} r_1 dr_1 d\phi_1 \right) e^{-\lambda_0 \pi R^2} (\lambda_0 \pi R^2) \\ &+ \int_0^{2\pi} \int_0^R r_1 dr_1 d\phi_1 \int_0^{2\pi} \int_{r_1}^R g(A_v^{(2+)}(\mathbf{p}^{(2)}; \mathbf{z}); \lambda) \lambda_0^2 e^{-\lambda_0 \pi r^2} r_2 dr_2 d\phi_2 \end{aligned} \quad (47)$$

$$\triangleq b^{(2+)}(\lambda, \mathbf{z}). \quad (48)$$

We now proceed to determine the conditions under which  $b^{(2+)}(\lambda, \mathbf{z})$  is a *good* approximation for  $b(\lambda, \mathbf{z})$ .

**Theorem 2.** Given  $\mathbf{z}$ ,  $b^{(2+)}(\lambda, \mathbf{z}) \geq b^{\text{ind}}(\lambda, \mathbf{z})$  over  $\{(\lambda, \mathbf{z}) : \lambda \mathbb{E}[A_v(\mathbf{z})|\mathbf{K}_2] \geq 3.3836\}$ , where  $\mathbf{K}_2$  denotes the event that there are at least two obstacles present in  $\mathcal{D}_o(R)$ .

*Proof:* By conditioning on  $\mathbf{K}_2$  and  $\mathbf{K}_2^c$ ,  $\mathbb{E}[A_v(\mathbf{z})]$  can be expressed as follows:

$$\mathbb{E}[A_v(\mathbf{z})] = \mathbb{E}[A_v(\mathbf{z})|\mathbf{K}_2^c] \mathbb{P}(\mathbf{K}_2^c) + \mathbb{E}[A_v(\mathbf{z})|\mathbf{K}_2] \mathbb{P}(\mathbf{K}_2). \quad (49)$$

Clearly,  $\mathbb{E}[A_v(\mathbf{z})|\mathbf{K}_2] \leq \mathbb{E}[A_v(\mathbf{z})|\mathbf{K}_2^c]$  as the average unshadowed area can only decrease as the number of obstacles increases. Since  $g(x; \lambda)$  is convex if and only if  $\lambda x \geq 2$ , the following holds, from Jensen's inequality, for  $\lambda \mathbb{E}[A_v(\mathbf{z})|\mathbf{K}_2^c] \geq \lambda \mathbb{E}[A_v(\mathbf{z})|\mathbf{K}_2] \geq 2$ ,

$$b^{\text{ind}}(\lambda, \mathbf{z}) = g(\mathbb{E}[A_v(\mathbf{z})]; \lambda) \quad (50)$$

$$= g(\mathbb{E}[A_v(\mathbf{z})|\mathbf{K}_2^c]\mathbb{P}(\mathbf{K}_2^c) + \mathbb{E}[A_v(\mathbf{z})|\mathbf{K}_2]\mathbb{P}(\mathbf{K}_2); \lambda) \quad (51)$$

$$\leq g(\mathbb{E}[A_v(\mathbf{z})|\mathbf{K}_2^c]; \lambda)\mathbb{P}(\mathbf{K}_2^c) + g(\mathbb{E}[A_v(\mathbf{z})|\mathbf{K}_2]; \lambda)\mathbb{P}(\mathbf{K}_2). \quad (52)$$

Furthermore, from Theorem 1, we have the following inequality for  $\lambda \mathbb{E}[A_v(\mathbf{z})|\mathbf{K}_2^c] \geq 3.3836$ ,

$$g(\mathbb{E}[A_v(\mathbf{z})|\mathbf{K}_2^c]; \lambda) \leq \mathbb{E}[g(A_v(\mathbf{z}); \lambda)|\mathbf{K}_2^c]. \quad (53)$$

By further conditioning  $\mathbf{K}_2$  on the obstacle locations,  $\mathbb{E}[A_v(\mathbf{z})|\mathbf{K}_2]$  can be expressed as follows:

$$\mathbb{E}[A_v(\mathbf{z})|\mathbf{K}_2] = \mathbb{E}_{\mathbf{p}^{(2)}}[A_{n2}(\mathbf{p}^{(2)}; \mathbf{z}) + \mathbb{E}[A_f(\mathbf{p}^{(k)}; \mathbf{z})|\mathbf{p}^{(2)}]]. \quad (54)$$

**Remark 3.**  $\mathbb{E}[A_v(\mathbf{z})|\mathbf{K}_2]$  can also be obtained by averaging the expression in (28) over  $k$ . The expression in (54) is an equivalent representation of the same quantity.

Again, from Theorem 1, the following inequality holds for  $\lambda \mathbb{E}[A_v(\mathbf{z})|\mathbf{K}_2] \geq 3.3836$

$$g(\mathbb{E}[A_v(\mathbf{z})|\mathbf{K}_2]; \lambda) = g(\mathbb{E}_{\mathbf{p}^{(2)}}[A_{n2}(\mathbf{p}^{(2)}; \mathbf{z}) + \mathbb{E}[A_f(\mathbf{p}^{(k)}; \mathbf{z})|\mathbf{p}^{(2)}]]; \lambda) \quad (55)$$

$$\leq \mathbb{E}_{\mathbf{p}^{(2)}}[g(A_{n2}(\mathbf{p}^{(2)}; \mathbf{z}) + \mathbb{E}[A_f(\mathbf{p}^{(k)}; \mathbf{z})|\mathbf{p}^{(2)}]; \lambda)]. \quad (56)$$

Thus, from (49)-(56), for  $\lambda \mathbb{E}[A_v(\mathbf{z})|\mathbf{K}_2^c] \geq \lambda \mathbb{E}[A_v(\mathbf{z})|\mathbf{K}_2] \geq 3.3836$ , we have

$$\begin{aligned} b^{\text{ind}}(\lambda, \mathbf{z}) &= g(\mathbb{E}[A_v(\mathbf{z})]; \lambda) \\ &\leq \mathbb{E}[g(A_v(\mathbf{z}); \lambda)|\mathbf{K}_2^c]\mathbb{P}(\mathbf{K}_2^c) + \mathbb{E}_{\mathbf{p}^{(2)}}[g(A_{n2}(\mathbf{p}^{(2)}; \mathbf{z}) + \mathbb{E}[A_f(\mathbf{p}^{(k)}; \mathbf{z})|\mathbf{p}^{(2)}]; \lambda)]\mathbb{P}(\mathbf{K}_2) \\ &= b^{(2+)}(\lambda, \mathbf{z}). \end{aligned} \quad (57)$$

■

**Theorem 3.** Given  $\mathbf{z}$  and  $\lambda$ ,  $b^{(2+)}(\lambda, \mathbf{z}) - b(\lambda, \mathbf{z}) \leq c(\lambda; \mathbf{z})$ , where  $c(\lambda; \mathbf{z}) \in (0, 1)$  is a decreasing function in  $\lambda$ .

*Proof:* Conditioning on  $\mathbf{K}_2$  and  $\mathbf{K}_2^c$ ,  $b(\lambda, \mathbf{z})$  and  $b^{(2+)}(\lambda, \mathbf{z})$  can be expressed as follows:

$$\begin{aligned} b(\lambda, \mathbf{z}) &= \mathbb{E}[g(A_v(\mathbf{z}); \lambda)|\mathbf{K}_2^c]\mathbb{P}(\mathbf{K}_2^c) + \mathbb{E}[g(A_v(\mathbf{z}); \lambda)|\mathbf{K}_2]\mathbb{P}(\mathbf{K}_2) \\ &= \mathbb{E}[g(A_v(\mathbf{z}); \lambda)|\mathbf{K}_2^c]\mathbb{P}(\mathbf{K}_2^c) + \mathbb{E}_{\mathbf{p}^{(2)}}[\mathbb{E}[g(A_{n2}(\mathbf{p}^{(2)}; \mathbf{z}) + A_f(\mathbf{p}^{(k)}; \mathbf{z}); \lambda)|\mathbf{p}^{(2)}]]\mathbb{P}(\mathbf{K}_2) \end{aligned} \quad (58)$$

$$b^{(2+)}(\lambda, \mathbf{z}) = \mathbb{E}[g(A_v(\mathbf{z}); \lambda) | \mathbf{K}_2^c] \mathbb{P}(\mathbf{K}_2^c) + \mathbb{E}_{\mathbf{p}^{(2)}}[g(A_{n2}(\mathbf{p}^{(2)}; \mathbf{z}) + \mathbb{E}[A_f(\mathbf{p}^{(k)}; \mathbf{z}) | \mathbf{p}^{(2)}]; \lambda)] \mathbb{P}(\mathbf{K}_2). \quad (59)$$

Similar to (32), the conditional expectation in (58), given  $\mathbf{p}^{(2)}$ , is over both  $k$  and  $\mathbf{p}^{(3:k)}$ . Let

$$g_1(\mathbf{p}^{(2)}; \lambda, \mathbf{z}) = \mathbb{E}[g(A_{n2}(\mathbf{p}^{(2)}; \mathbf{z}) + A_f(\mathbf{p}^{(k)}; \mathbf{z}); \lambda) | \mathbf{p}^{(2)}] \quad (60)$$

$$g_2(\mathbf{p}^{(2)}; \lambda, \mathbf{z}) = g(A_{n2}(\mathbf{p}^{(2)}; \mathbf{z}) + \mathbb{E}[A_f(\mathbf{p}^{(k)}; \mathbf{z}) | \mathbf{p}^{(2)}]; \lambda) \quad (61)$$

$$\mathcal{R}_1(\lambda; \mathbf{z}) := \{\mathbf{p}^{(2)} \in \mathcal{D}_o(R) \times \mathcal{D}_o(R) : g_1(\mathbf{p}^{(2)}; \lambda, \mathbf{z}) \geq g_2(\mathbf{p}^{(2)}; \lambda, \mathbf{z}), r_1 \leq r_2\} \quad (62)$$

$$\mathcal{R}_2(\lambda; \mathbf{z}) := \{\mathbf{p}^{(2)} \in \mathcal{D}_o(R) \times \mathcal{D}_o(R) : g_1(\mathbf{p}^{(2)}; \lambda, \mathbf{z}) < g_2(\mathbf{p}^{(2)}; \lambda, \mathbf{z}), r_1 \leq r_2\} \quad (63)$$

$$\mathcal{F}_1(\lambda; \mathbf{z}) := \{\mathbf{p}^{(2)} \in \mathcal{D}_o(R) \times \mathcal{D}_o(R) : A_{n2}(\mathbf{p}^{(2)}; \mathbf{z}) \geq 2/\lambda, r_1 \leq r_2\} \quad (64)$$

$$\mathcal{F}_2(\lambda; \mathbf{z}) := \{\mathbf{p}^{(2)} \in \mathcal{D}_o(R) \times \mathcal{D}_o(R) : A_{n2}(\mathbf{p}^{(2)}; \mathbf{z}) < 2/\lambda, r_1 \leq r_2\} \quad (65)$$

Since  $g(x; \lambda)$  is convex whenever  $\lambda x \geq 2$ , it follows that  $g(\cdot; \lambda)$  is convex over the set of  $A_{n2}(\mathbf{p}^{(2)}; \mathbf{z})$  resulting from  $\mathcal{F}_1$ . Hence, from Jensen's inequality,  $\mathcal{F}_1 \subseteq \mathcal{R}_1$ . As a result,  $\mathcal{F}_2 \supseteq \mathcal{R}_2$ , since  $\mathcal{R}_1 \cup \mathcal{R}_2 = \mathcal{F}_1 \cup \mathcal{F}_2$ . Hence, from (58)-(65),

$$b^{(2+)}(\lambda, \mathbf{z}) - b(\lambda, \mathbf{z}) = \mathbb{P}(\mathbf{K}_2) \left( \int_{\mathcal{R}_1(\lambda; \mathbf{z})} (g_2(\mathbf{p}^{(2)}; \lambda, \mathbf{z}) - g_1(\mathbf{p}^{(2)}; \lambda, \mathbf{z})) f(\mathbf{p}^{(2)}) d\mathbf{p}^{(2)} + \int_{\mathcal{R}_2(\lambda; \mathbf{z})} (g_2(\mathbf{p}^{(2)}; \lambda, \mathbf{z}) - g_1(\mathbf{p}^{(2)}; \lambda, \mathbf{z})) f(\mathbf{p}^{(2)}) d\mathbf{p}^{(2)} \right), \quad (66)$$

$$(67)$$

where  $f(\mathbf{p}^{(2)})$  denotes the pdf of  $\mathbf{p}^{(2)}$ . Since the integral over  $\mathcal{R}_1(\lambda; \mathbf{z})$  is non-positive, we have

$$b^{(2+)}(\lambda, \mathbf{z}) - b(\lambda, \mathbf{z}) \leq \mathbb{P}(\mathbf{K}_2) \int_{\mathcal{R}_2(\lambda; \mathbf{z})} (g_2(\mathbf{p}^{(2)}; \lambda, \mathbf{z}) - g_1(\mathbf{p}^{(2)}; \lambda, \mathbf{z})) f(\mathbf{p}^{(2)}) d\mathbf{p}^{(2)} \quad (68)$$

$$\leq \mathbb{P}(\mathbf{K}_2) \int_{\mathcal{F}_2(\lambda; \mathbf{z})} (g_2(\mathbf{p}^{(2)}; \lambda, \mathbf{z}) - g_1(\mathbf{p}^{(2)}; \lambda, \mathbf{z})) f(\mathbf{p}^{(2)}) d\mathbf{p}^{(2)} \quad (69)$$

$$\leq \mathbb{P}(\mathbf{K}_2) \left( 1 - \min_{\mathbf{u} \in \mathcal{F}_2(\lambda; \mathbf{z})} g_1(\mathbf{u}; \lambda) \right) \int_{\mathcal{F}_2(\lambda; \mathbf{z})} f(\mathbf{p}^{(2)}) d\mathbf{p}^{(2)} \quad (70)$$

$$:= c(\lambda; \mathbf{z}), \quad (71)$$

where  $c(\lambda; \mathbf{z}) := \mathbb{P}(\mathbf{K}_2) \left( 1 - \min_{\mathbf{u} \in \mathcal{F}_2(\lambda; \mathbf{z})} g_1(\mathbf{u}; \lambda) \right) \mathbb{P}(\mathbf{p}^{(2)} \in \mathcal{F}_2(\lambda; \mathbf{z}))$  is non-negative and decreasing in  $\lambda$  and is bounded above by one.  $\blacksquare$

**Remark 4.** From Theorems 2 and 3,  $b^{\text{ind}}(\lambda, \mathbf{z}) \leq b^{(2+)}(\lambda, \mathbf{z}) \leq b(\lambda, \mathbf{z}) + c(\lambda; \mathbf{z})$ , for sufficiently large  $\lambda$ . In other words,  $b^{(2+)}(\lambda, \mathbf{z})$  better approximates  $b(\lambda, \mathbf{z})$  as  $\lambda$  increases.

To summarize, it is intuitive that obstacles which are closer to the typical target induce greater blocking correlation, with the extent of correlation decreasing with distance. Hence, by taking into account the impact of correlated blocking due to the nearest two obstacles,  $b^{(2+)}(\lambda, \mathbf{z})$  achieves a reasonable trade-off between accuracy and tractability.

## VI. NUMERICAL RESULTS

We set  $R = 10\text{m}$  throughout and for each  $(\lambda, \mathbf{z})$ , the following cases were evaluated: (i)  $b(\lambda, \mathbf{z})$ , obtained by averaging over  $10^6$  Monte-Carlo simulations, (ii)  $b^{(2+)}(\lambda, \mathbf{z})$ , given by (47), and (iii)  $b^{\text{ind}}(\lambda, \mathbf{z})$ . For fixed  $\mathbf{z}$ , the blind-spot probability curves corresponding to these four cases are plotted in Fig. 7, as a function of  $\lambda$ . Since the nearest two-obstacle approximation captures some of the blocking correlation,  $b^{(2+)}(\lambda, \mathbf{z})$  approximates  $b(\lambda, \mathbf{z})$  more closely than  $b^{\text{ind}}(\lambda, \mathbf{z})$ . The approximation error can be further reduced by considering the blocking correlation beyond second nearest obstacle; however, this comes at the expense of tractability as we would have to deal with more complex overlaps involving the shadowed regions. From a design perspective, Fig. 7 can be used to determine the anchor intensity,  $\lambda$ , such that  $b(\lambda, \mathbf{z}) \approx b^{(2+)}(\lambda, \mathbf{z}) \leq \mu$ .

For fixed  $\lambda$  and  $\lambda_0$ , the effect of obstacle length,  $L$ , on the blind-spot probability is shown in Fig 8. As expected, the gap between  $b^{\text{ind}}(\lambda, \mathbf{z})$  and  $b(\lambda, \mathbf{z})$  increases with  $L$ , since the extent of correlated blocking increases monotonically with  $L$ , while  $b^{(2+)}(\lambda, \mathbf{z})$  better approximates  $b(\lambda, \mathbf{z})$  by effectively capturing most of the blocking correlation.

## VII. SUMMARY

In this paper, we set out to analyze the impact of correlated blocking on the blind-spot probability of a localization network. The anchor locations were modeled using a homogeneous PPP and the obstacle locations and shapes using a germ-grain model. Under these conditions, we characterized the blind-spot probability as a function of the pdf of the unshadowed area. Furthermore, we showed that the blind-spot probability under the independent anchor blocking assumption depends only on the mean unshadowed area, instead of the entire probability distribution, and derived the conditions under which the independent blocking assumption underestimates the true blind-spot probability. Since the pdf of the unshadowed area is difficult to characterize

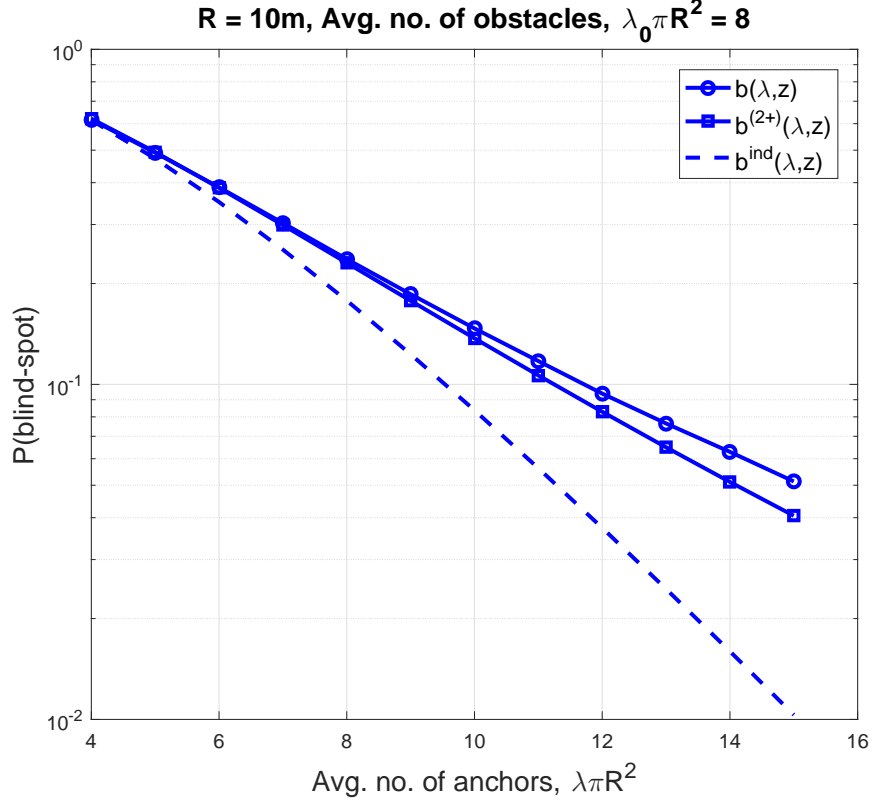


Fig. 7: The nearest two-obstacle approximation yields a tighter lower bound to the true blind-spot probability.

in closed-form, we derived an approximate expression for the blind-spot probability by formulating the *nearest two-obstacle approximation*, which captures the blocking correlation up to the second nearest obstacle and assumes independent blocking due to farther obstacles. This yields a reasonable trade-off between accuracy and tractability, wherein our approximation is more accurate than the independent blocking assumption in estimating the true blind-spot probability, as the anchor intensity increases. As a result, our approximation provides better design insights, such as the intensity with which anchors need to be deployed so that the blind-spot probability over the entire region is less than a threshold,  $\mu$ .

Finally, as one of the first works that, to the best of our knowledge, takes into account correlated blocking, the techniques developed in this paper provide valuable insights into the modeling and analysis of the impact of correlated blocking in not only localization systems, but also in other applications where correlated blocking is an increasingly relevant, yet poorly investigated, phenomenon, such as mm-wave communication systems.

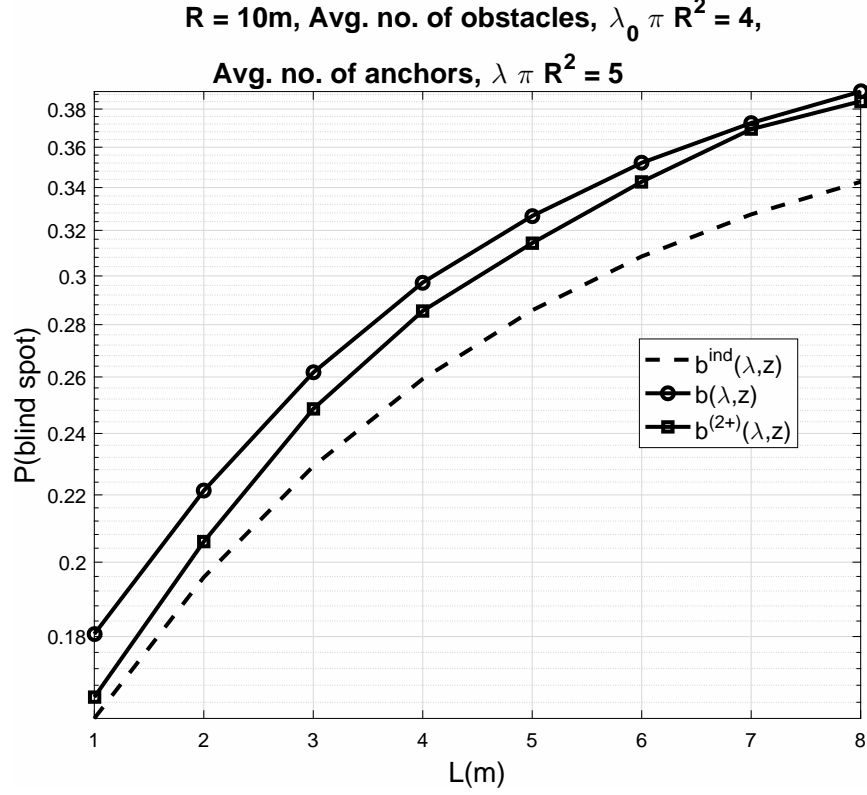


Fig. 8: Larger obstacles induce greater blocking correlation, as a result of which the gap between the  $b(\lambda, z)$  and  $b^{\text{ind}}(\lambda, z)$  increases with  $L$ , for fixed values of the other parameters.

## APPENDIX

### A. Proof of Lemma 1

The unshaded area,  $A_v(\mathbf{z})$ , can be expressed as follows:

$$A_v(\mathbf{z}) = \int_0^{2\pi} \int_0^R V(\mathbf{p}; \mathbf{z}) r dr d\phi \quad (72)$$

$$\therefore \mathbb{E}[A_v(\mathbf{z})] = \int_0^{2\pi} \int_0^R \mathbb{E}[V(\mathbf{p}; \mathbf{z})] r dr d\phi = \int_0^{2\pi} \int_0^R \mathbb{P}(V(\mathbf{p}; \mathbf{z}) = 1) r dr d\phi = 2\pi \int_0^R \mathbb{P}(V(\mathbf{p}; \mathbf{z}) = 1) r dr, \quad (73)$$

where (73) follows from the spherical symmetry of the system model considered in Section II.

For independent anchor blocking, the unblocked anchors can be viewed as a point process obtained by independently sampling the anchor PPP, where the sampling probability of an anchor at  $\mathbf{p} \in \mathcal{D}_o(R)$ , with respect to the typical target, equals  $\mathbb{P}(V(\mathbf{p}; \mathbf{z}) = 1)$ . As a result, the unblocked

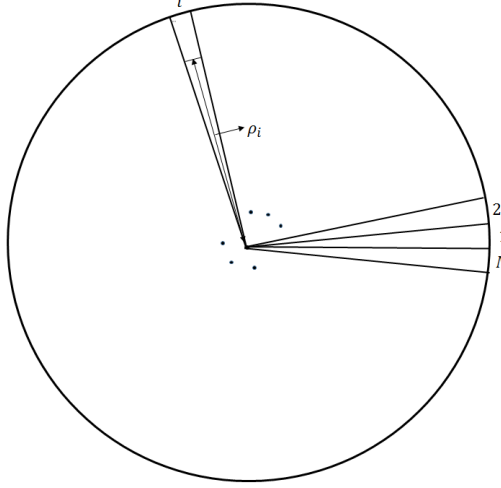


Fig. 9: For independent blocking, the distance up to which LoS exists in each of the slices form a collection of i.i.d random variables.

anchors to the typical target form a non-homogeneous PPP whose intensity,  $\lambda_{\text{ind}}(\mathbf{p}; \mathbf{z})$ , is given by

$$\lambda_{\text{ind}}(\mathbf{p}; \mathbf{z}) = \lambda \mathbb{P}(V(\mathbf{p}; \mathbf{z}) = 1). \quad (74)$$

For a non-homogeneous anchor PPP with intensity  $\lambda_{\text{ind}}(\mathbf{p}; \mathbf{z})$ , the number of anchors over a circle of radius  $R$  has a Poisson distribution with mean  $\Lambda(\lambda, \mathbf{z})$ , given by

$$\Lambda(\lambda, \mathbf{z}) = \int_0^{2\pi} \int_0^R \lambda_{\text{ind}}(\mathbf{p}; \mathbf{z}) r dr d\phi = \lambda \mathbb{E}[A_v(\mathbf{z})], \quad (75)$$

where (75) is obtained from (73). Hence, the blind-spot probability due to independent anchor blocking is given by

$$\begin{aligned} b^{\text{ind}}(\lambda, \mathbf{z}) &= e^{-\Lambda(\lambda, \mathbf{z})} \left( 1 + \Lambda(\lambda, \mathbf{z}) + \frac{(\Lambda(\lambda, \mathbf{z}))^2}{2} \right) \\ &= e^{-\lambda \mathbb{E}[A_v(\mathbf{z})]} \left( 1 + \lambda \mathbb{E}[A_v(\mathbf{z})] + \frac{(\lambda \mathbb{E}[A_v(\mathbf{z})])^2}{2} \right) \\ &= g(\mathbb{E}[A_v(\mathbf{z})]; \lambda). \end{aligned} \quad (76)$$

■

### B. Proof of Corollary 1

For independent anchor blocking, the concentration of  $f_{A_v(\mathbf{z})}(\cdot)$  around  $\mathbb{E}[A_v(\mathbf{z})]$  can be explained using the law of large numbers (LLN) [24]. Suppose  $\mathcal{D}_o(R)$  is split into  $N$  slices, as



shown in Fig. 9. For large  $N$ , the unshadowed region in the  $i$ -th slice can be approximated by a triangle whose area  $A_i(\mathbf{z})$ , is expressed as follows,

$$A_i(\mathbf{z}) = \frac{1}{2} \rho_i(\mathbf{z}) \left( \rho_i(\mathbf{z}) \frac{2\pi}{N} \right) = \frac{\pi \rho_i^2(\mathbf{z})}{N}, \quad (77)$$

where  $\rho_i(\mathbf{z}) \in [0, R]$  is the distance up to which LoS exists for the  $i$ -th slice ( $i = 1, \dots, N$ ). The pdf of  $\rho_i(\mathbf{z})$ , denoted by  $f_{\rho_i(\mathbf{z})}(r)$ , is obtained from its tail probability in the following manner:

$$f_{\rho_i(\mathbf{z})}(r) = -\frac{d}{dr} \mathbb{P}(\rho_i(\mathbf{z}) > r) + \mathbb{P} \left( V \left( \left( R, \frac{2\pi i}{N} \right); \mathbf{z} \right) = 1 \right) \delta(r - R), \quad (78)$$

$$\text{where } \mathbb{P}(\rho_i(\mathbf{z}) > r) = \begin{cases} \mathbb{P} \left( V \left( \left( r, \frac{2\pi i}{N} \right); \mathbf{z} \right) = 1 \right), & r \in [0, R) \\ 0, & \text{else,} \end{cases} \quad (79)$$

and  $V((r, 2\pi/N); \mathbf{z})$  is defined in (1). Therefore,

$$A_v(\mathbf{z}) = \sum_{i=1}^N A_i(\mathbf{z}) = \pi \sum_{i=1}^N \frac{\rho_i^2(\mathbf{z})}{N}. \quad (80)$$

$\{\rho_i(\mathbf{z}) : i = 1, \dots, N\}$  form a collection of i.i.d random variables if independent anchor blocking is assumed. Hence, by LLN,

$$\begin{aligned} A_v(\mathbf{z}) &\xrightarrow{\text{w.p.1}} \pi \mathbb{E}[\rho_i^2(\mathbf{z})] \\ &= \pi \int_0^R r^2 f_{\rho_i(\mathbf{z})}(r) dr \\ &= \pi \int_0^R r^2 \left( -\frac{d}{dr} \mathbb{P} \left( V \left( \left( r, \frac{2\pi i}{N} \right); \mathbf{z} \right) = 1 \right) + \mathbb{P} \left( V \left( \left( R, \frac{2\pi i}{N} \right); \mathbf{z} \right) = 1 \right) \delta(r - R) \right) dr \\ &\quad (81) \end{aligned}$$

$$\begin{aligned} &= \pi \left[ -r^2 \mathbb{P} \left( V \left( \left( r, \frac{2\pi i}{N} \right); \mathbf{z} \right) = 1 \right) \Big|_0^R + \int_0^R 2r \mathbb{P} \left( V \left( \left( r, \frac{2\pi i}{N} \right); \mathbf{z} \right) = 1 \right) dr \right. \\ &\quad \left. + R^2 \mathbb{P} \left( V \left( \left( R, \frac{2\pi i}{N} \right); \mathbf{z} \right) = 1 \right) \right] \\ &= \mathbb{E}[A_v(\mathbf{z})], \quad (82) \end{aligned}$$

where  $\xrightarrow{\text{w.p.1}}$  denotes convergence with probability one (or almost-sure convergence). The expression in (81) is obtained by integrating by parts and (82) follows from (73) in Appendix A. Hence,  $f_{A_v(\mathbf{z})}(x) = \delta(x - \mathbb{E}[A_v](\mathbf{z}))$  for independent anchor blocking.

### C. Proof of Lemma 2

An obstacle with mid-point at  $(\rho, \beta)$  (in polar coordinates) can block the LoS path between the typical target and an anchor at  $\mathbf{p} \in \mathcal{D}_o(R)$  if and only if the following conditions are satisfied (see Fig. 10)

$$0 \leq \rho \tan |\beta - \phi| \leq L/2 \quad (83)$$

$$0 \leq \rho \sec |\beta - \phi| \leq r. \quad (84)$$

Hence,  $V(\mathbf{p}; \mathbf{z}) = 1$  is unblocked if and only if there are no obstacle mid-points in the set  $S_V(\mathbf{p}; \mathbf{z}) = S_{V_1}(\mathbf{p}; \mathbf{z}) \cap S_{V_2}(\mathbf{p}; \mathbf{z})$  (Fig. 10), where

$$S_{V_1}(\mathbf{p}; \mathbf{z}) = \{(\rho, \beta) \in \mathbb{R}^2 : 0 \leq \rho \tan |\beta - \phi| \leq L/2\} \quad (85)$$

$$S_{V_2}(\mathbf{p}; \mathbf{z}) = \{(\rho, \beta) \in \mathbb{R}^2 : 0 \leq \rho \sec |\beta - \phi| \leq r\}. \quad (86)$$

From (85) and (86), the azimuthal end-points of  $S_V(\mathbf{p}; \mathbf{z})$  at a radial distance  $\rho \in [0, r]$  are given by  $\phi \pm \min\left(\arctan\left(\frac{L}{2\rho}\right), \arccos\left(\frac{\rho}{r}\right)\right)$ . Therefore,

$$\mathbb{P}(V(\mathbf{p}; \mathbf{z}) = 1) = \mathbb{P}(\text{no obstacle mid-point in } S_V(\mathbf{p}; \mathbf{z})) = e^{-\lambda_0 \nu_2(S_V(\mathbf{p}; \mathbf{z}))} \quad (87)$$

$$\begin{aligned} \text{where } \nu_2(S_V(\mathbf{p}; \mathbf{z})) &= \int_0^r \int_{\phi - \min(\arctan(L/(2\rho)), \arccos(\rho/r))}^{\phi + \min(\arctan(L/(2\rho)), \arccos(\rho/r))} \rho d\phi d\rho \\ &= 2 \int_0^r \rho \min(\arctan(L/(2\rho)), \arccos(\rho/r)) d\rho. \end{aligned} \quad (88)$$

Substituting (87) and (88) in (73) completes the proof.  $\blacksquare$

### D. Proof of Lemma 3

Suppose there exists an overlap between  $\mathcal{A}_{\text{sh}}(\mathbf{p}_2; \mathbf{z})$  and  $\mathcal{A}_{\text{sh}}(\mathbf{p}_1; \mathbf{z})$ . Then, let  $\epsilon(\mathbf{p}^{(2)}; \mathbf{z})$  denote the azimuthal width of  $\mathcal{A}_{\text{sh}}(\mathbf{p}_2; \mathbf{z}) \cap \mathcal{A}_{\text{sh}}(\mathbf{p}_1; \mathbf{z})$ . The feasible scenarios for the end-points of the intervals  $\mathcal{I}(\mathbf{p}_1; \mathbf{z})$  and  $\mathcal{I}(\mathbf{p}_2; \mathbf{z})$  are as follows:

- Case 1:  $l(\mathbf{p}_1; \mathbf{z}) \leq u(\mathbf{p}_1; \mathbf{z})$  and  $l(\mathbf{p}_2; \mathbf{z}) \leq u(\mathbf{p}_2; \mathbf{z})$

This corresponds to when  $\{(r, 0) : 0 \leq r \leq R\} \notin \mathcal{A}_{\text{sh}}(\mathbf{p}_1; \mathbf{z}) \cup \mathcal{A}_{\text{sh}}(\mathbf{p}_2; \mathbf{z})$  (Fig. 11a). For an overlap to occur between  $\mathcal{A}_{\text{sh}}(\mathbf{p}_2; \mathbf{z})$  and  $\mathcal{A}_{\text{sh}}(\mathbf{p}_1; \mathbf{z})$ , one of the following conditions must be satisfied:

- $l(\mathbf{p}_1; \mathbf{z}) \leq l(\mathbf{p}_2; \mathbf{z}) < u(\mathbf{p}_1; \mathbf{z})$  (top, Fig. 11a).
- $l(\mathbf{p}_2; \mathbf{z}) \leq l(\mathbf{p}_1; \mathbf{z}) < u(\mathbf{p}_2; \mathbf{z})$  (bottom, Fig. 11a).

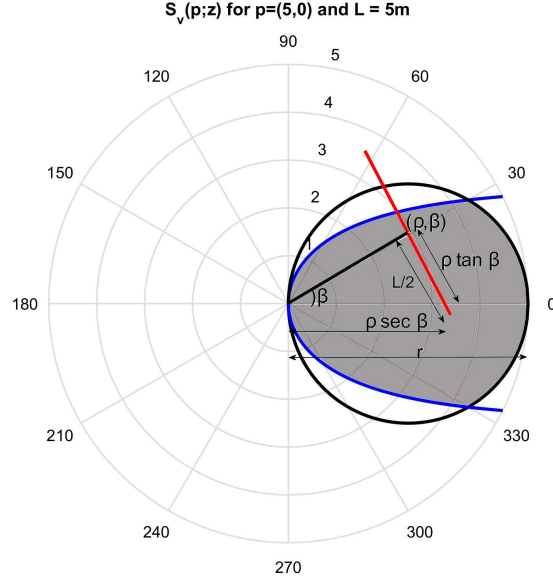
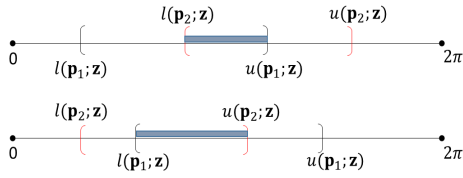
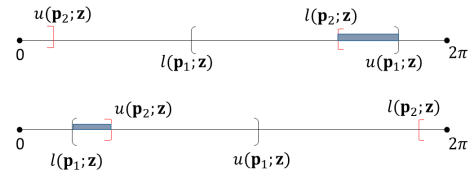


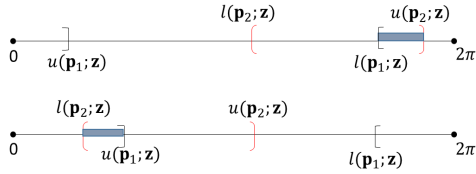
Fig. 10: For  $\mathbf{p} = (5, 0)$ , the region enclosed by the blue curve corresponds to  $S_{V_1}(\mathbf{p}; \mathbf{z}) = \{(\rho, \beta) \in \mathbb{R}^2 : 0 \leq \rho \tan |\beta - \phi| \leq L/2\}$ . Similarly, the region enclosed by the black curve corresponds to  $S_{V_2}(\mathbf{p}; \mathbf{z}) = \{(\rho, \beta) \in \mathbb{R}^2 : 0 \leq \rho \sec |\beta - \phi| \leq r\}$ . Hence, the LoS path to  $\mathbf{o}$  is unblocked if and only if there is no obstacle mid-point in the shaded region, which corresponds to  $S_V(\mathbf{p}; \mathbf{z}) = S_{V_1}(\mathbf{p}; \mathbf{z}) \cap S_{V_2}(\mathbf{p}; \mathbf{z})$ .



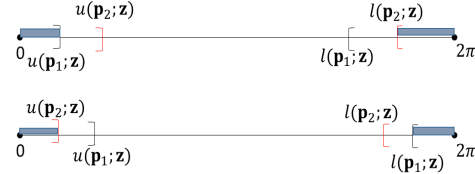
(a) Case 1



(b) Case 2



(c) Case 3



(d) Case 4

Fig. 11: Feasible overlap situations between  $\mathcal{A}_{\text{sh}}(\mathbf{p}_1; \mathbf{z})$  and  $\mathcal{A}_{\text{sh}}(\mathbf{p}_2; \mathbf{z})$  in the azimuth coordinate. The size of the interval shaded grey denotes  $\epsilon(\mathbf{p}^{(2)}; \mathbf{z})$ .

Hence,

$$\epsilon(\mathbf{p}^{(2)}; \mathbf{z}) = \min(u(\mathbf{p}_1; \mathbf{z}), u(\mathbf{p}_2; \mathbf{z})) - \max(l(\mathbf{p}_1; \mathbf{z}), l(\mathbf{p}_2; \mathbf{z})). \quad (89)$$

- Case 2:  $l(\mathbf{p}_1; \mathbf{z}) \leq u(\mathbf{p}_1; \mathbf{z})$  and  $l(\mathbf{p}_2; \mathbf{z}) > u(\mathbf{p}_2; \mathbf{z})$  This corresponds to when  $\{(r, 0) : 0 \leq r \leq R\} \notin \mathcal{A}_{\text{sh}}(\mathbf{p}_1; \mathbf{z})$  and  $\{(r, 0) : 0 \leq r \leq R\} \in \mathcal{A}_{\text{sh}}(\mathbf{p}_2; \mathbf{z})$  (Fig. 11b). For an overlap to occur, exactly one of the following conditions must be satisfied:

- a)  $u(\mathbf{p}_2; \mathbf{z}) < l(\mathbf{p}_1; \mathbf{z}) < l(\mathbf{p}_2; \mathbf{z}) \leq u(\mathbf{p}_1; \mathbf{z})$  (top, Fig.11b).
- b)  $u(\mathbf{p}_2; \mathbf{z}) > l(\mathbf{p}_1; \mathbf{z})$  (bottom, Fig.11b).

Hence,

$$\epsilon(\mathbf{p}^{(2)}; \mathbf{z}) = \max(u(\mathbf{p}_2; \mathbf{z}) - l(\mathbf{p}_1; \mathbf{z}), u(\mathbf{p}_1; \mathbf{z}) - l(\mathbf{p}_2; \mathbf{z})). \quad (90)$$

- Case 3:  $l(\mathbf{p}_1; \mathbf{z}) > u(\mathbf{p}_1; \mathbf{z})$  and  $l(\mathbf{p}_2; \mathbf{z}) \leq u(\mathbf{p}_2; \mathbf{z})$  This corresponds to when  $\{(r, 0) : 0 \leq r \leq R\} \in \mathcal{A}_{\text{sh}}(\mathbf{p}_1; \mathbf{z})$  and  $\{(r, 0) : 0 \leq r \leq R\} \notin \mathcal{A}_{\text{sh}}(\mathbf{p}_2; \mathbf{z})$  (Fig. 11c). For an overlap to occur, exactly one of the following conditions must be satisfied:

- a)  $l(\mathbf{p}_2; \mathbf{z}) < u(\mathbf{p}_1; \mathbf{z})$  (top, Fig. 11c).
- b)  $u(\mathbf{p}_2; \mathbf{z}) > l(\mathbf{p}_1; \mathbf{z})$  (bottom, Fig. 11c).

Hence,

$$\epsilon(\mathbf{p}^{(2)}; \mathbf{z}) = \max(u(\mathbf{p}_2; \mathbf{z}) - l(\mathbf{p}_1; \mathbf{z}), u(\mathbf{p}_1; \mathbf{z}) - l(\mathbf{p}_2; \mathbf{z})). \quad (91)$$

- Case 4:  $l(\mathbf{p}_1; \mathbf{z}) > u(\mathbf{p}_1; \mathbf{z})$  and  $l(\mathbf{p}_2; \mathbf{z}) > u(\mathbf{p}_2; \mathbf{z})$  This corresponds to when  $\{(r, 0) : 0 \leq r \leq R\} \in \mathcal{A}_{\text{sh}}(\mathbf{p}_1; \mathbf{z}) \cap \mathcal{A}_{\text{sh}}(\mathbf{p}_2; \mathbf{z})$  (Fig. 11d). For an overlap to occur, one of the following conditions must be satisfied:

- a)  $l(\mathbf{p}_1; \mathbf{z}) < l(\mathbf{p}_2; \mathbf{z})$  (top, Fig. 11d).
- b)  $u(\mathbf{p}_1; \mathbf{z}) > u(\mathbf{p}_2; \mathbf{z})$  (bottom, Fig. 11d)

Hence,

$$\epsilon(\mathbf{p}^{(2)}; \mathbf{z}) = 2\pi - (\max(l(\mathbf{p}_1; \mathbf{z}), l(\mathbf{p}_2; \mathbf{z})) - \min(u(\mathbf{p}_1; \mathbf{z}), u(\mathbf{p}_2; \mathbf{z}))). \quad (92)$$

From the expressions in (89)-(92), it is easily seen that  $\epsilon(\mathbf{p}^{(2)}; \mathbf{z})$  is negative if  $\mathcal{A}_{\text{sh}}(\mathbf{p}_1; \mathbf{z}) \cap \mathcal{A}_{\text{sh}}(\mathbf{p}_2; \mathbf{z}) = \emptyset$ . Hence, from the above cases, the fraction of  $\mathcal{A}_{\text{sh}}(\mathbf{p}_2; \mathbf{z})$  that overlaps with  $\mathcal{A}_{\text{sh}}(\mathbf{p}_1; \mathbf{z})$  is given by,

$$\alpha(\mathbf{p}^{(2)}; \mathbf{z}) = \max\left(0, \frac{\epsilon(\mathbf{p}^{(2)}; \mathbf{z})}{\theta(\mathbf{p}_2; \mathbf{z})}\right), \quad (93)$$

$$\text{where } \epsilon(\mathbf{p}^{(2)}; \mathbf{z}) = \begin{cases} \min(u(\mathbf{p}_1; \mathbf{z}), u(\mathbf{p}_2; \mathbf{z})) - \max(l(\mathbf{p}_1; \mathbf{z}), l(\mathbf{p}_2; \mathbf{z})), & \text{if} \\ \quad l(\mathbf{p}_1; \mathbf{z}) \leq u(\mathbf{p}_1; \mathbf{z}), l(\mathbf{p}_2; \mathbf{z}) \leq u(\mathbf{p}_2; \mathbf{z}) \\ 2\pi - (\max(l(\mathbf{p}_1; \mathbf{z}), l(\mathbf{p}_2; \mathbf{z})) - \min(u(\mathbf{p}_1; \mathbf{z}), u(\mathbf{p}_2; \mathbf{z}))), & \text{if} \\ \quad l(\mathbf{p}_1; \mathbf{z}) > u(\mathbf{p}_1; \mathbf{z}), l(\mathbf{p}_2; \mathbf{z}) > u(\mathbf{p}_2; \mathbf{z}) \\ \max(u(\mathbf{p}_2; \mathbf{z}) - l(\mathbf{p}_1; \mathbf{z}), u(\mathbf{p}_1; \mathbf{z}) - l(\mathbf{p}_2; \mathbf{z})), & \text{else.} \end{cases} \quad (94)$$

■

### E. Proof of Lemma 4

Let  $\mathcal{A}_{\text{out}}(\mathbf{p}^{(2)}; \mathbf{z}) = \{(r, \phi) \in \mathcal{D}_{\text{o}}(R) : r > r_2, \phi \notin \mathcal{I}(\mathbf{p}_1; \mathbf{z}) \cup \mathcal{I}(\mathbf{p}_2; \mathbf{z})\} \supseteq \mathcal{V}_{\text{out}}(\mathbf{p}^{(k)}; \mathbf{z})$ . Similar to (73), we have

$$\mathbb{E}[\nu_2(\mathcal{V}_{\text{out}}(\mathbf{p}^{(k)}; \mathbf{z})) | \mathbf{p}^{(2)}] = \int_{\mathbf{p} \in \mathcal{A}_{\text{out}}(\mathbf{p}^{(2)}; \mathbf{z})} \mathbb{P}(V(\mathbf{p}; \mathbf{z}) = 1) r dr d\phi. \quad (95)$$

Due to rotational symmetry, the integral in (95) does not depend on azimuthal coordinate,  $\phi$ . Hence,

$$\mathbb{E}[\nu_2(\mathcal{V}_{\text{out}}(\mathbf{p}^{(k)}; \mathbf{z})) | \mathbf{p}^{(2)}] = \varphi_{\text{span}}(\mathcal{A}_{\text{out}}(\mathbf{p}^{(2)}; \mathbf{z})) \int_{r_2}^R \mathbb{P}(V(\mathbf{p}; \mathbf{z}) = 1) r dr, \quad (96)$$

$$\text{where } \varphi_{\text{span}}(\mathcal{A}_{\text{out}}(\mathbf{p}^{(2)}; \mathbf{z})) = 2\pi - \theta(\mathbf{p}_1; \mathbf{z}) - (1 - \alpha(\mathbf{p}^{(2)}; \mathbf{z}))\theta(\mathbf{p}_2; \mathbf{z}). \quad (97)$$

In (97),  $\varphi_{\text{span}}(\mathcal{A}_{\text{out}}(\mathbf{p}^{(2)}; \mathbf{z}))$  denotes the azimuthal width of  $\mathcal{A}_{\text{out}}(\mathbf{p}^{(2)}; \mathbf{z})$ . Substituting (87) and (88) in (95), we get the desired result. ■

## REFERENCES

- [1] S. Aditya, A. F. Molisch, H. S. Dhillon, H. Behairy, and N. Rabeah, “Blind-spot analysis of localization networks using second-order blocking statistics,” in *Intl. Conf. on Ubiquitous Wireless Broadband (ICUWB)*, Oct 2016.
- [2] S. Steineger, M. Neun, A. Edwardes, and B. Lenz, “Foundations of location based services,” 2006. [Online]. Available: [http://www.e-cartouche.ch/content\\_reg/cartouche/LBSbasics/en/text/LBSbasics.pdf](http://www.e-cartouche.ch/content_reg/cartouche/LBSbasics/en/text/LBSbasics.pdf)
- [3] A. Lo, L. Xia, I. Niemegeers, T. Bauge, M. Russell, and D. Harmer, “EUROPCOM - an Ultra-Wideband (UWB)-based ad hoc network for emergency applications,” in *Proc. of IEEE VTC Vehicular Technology Conference, Spring*, May 2008, pp. 6–10.
- [4] M. J. Murrian, C. W. Gonzalez, T. E. Humphreys, K. M. Pesyna, Jr., D. P. Shepard, and A. J. Kerns, “Low-cost precise positioning for automated vehicles,” *GPS World*, Sept. 2016.
- [5] K. Witrals, P. Meissner, E. Leitinger, Y. Shen, C. Gustafson, F. Tufvesson, K. Haneda, D. Dardari, A. F. Molisch, A. Conti, and M. Z. Win, “High-accuracy localization for assisted living: 5G systems will turn multipath channels from foe to friend,” *IEEE Signal Process. Mag.*, vol. 33, no. 2, pp. 59–70, March 2016.

- [6] D. Dardari and R. D'Errico, "Passive ultrawide bandwidth RFID," in *Proc. of IEEE Global Telecommunications Conf. (GLOBECOM)*, Nov 2008, pp. 1–6.
- [7] D. Dardari, R. D. Errico, C. Roblin, A. Sibille, and M. Z. Win, "Ultrawide bandwidth RFID: The next generation?" *Proc. IEEE*, vol. 98, no. 9, pp. 1570–1582, 2010.
- [8] N. Decarli, F. Guidi, and D. Dardari, "A novel joint RFID and radar sensor network for passive localization: Design and performance bounds," *IEEE J. Sel. Topics Signal Process.*, vol. 8, no. 1, pp. 80–95, Feb 2014.
- [9] S. Gezici, Z. Tian, G. Giannakis, H. Kobayashi, A. F. Molisch, H. Poor, and Z. Sahinoglu, "Localization via ultra-wideband radios: a look at positioning aspects for future sensor networks," *IEEE Signal Process. Mag.*, vol. 22, no. 4, pp. 70–84, July 2005.
- [10] Z. Ebrahimian and R. A. Scholtz, "Receiver sites for accurate indoor position location systems," in *IEEE-ACES Conf. on Wireless Comm. and Applied Comp. Electromagnetics*, April 2005.
- [11] H. González-Banos and J. C. Latombe, "A randomized art-gallery algorithm for sensor placement," in *Proc. 17th Annual Symp. on Comp. Geometry*, ser. SCG '01. ACM, 2001, pp. 232–240.
- [12] J. Schloemann, H. S. Dhillon, and R. M. Buehrer, "Towards a tractable analysis of localization fundamentals in cellular networks," *IEEE Trans. Wireless Commun.*, vol. 15, no. 3, pp. 1768–1782, March 2016.
- [13] —, "A tractable analysis of the improvement in unique localizability through collaboration," *IEEE Trans. Wireless Commun.*, vol. 15, no. 6, pp. 3934–3948, June 2016.
- [14] T. Bai, R. Vaze, and R. W. Heath Jr., "Analysis of blockage effects on urban cellular networks," *IEEE Trans. Wireless Commun.*, vol. 13, no. 9, pp. 5070–5083, Sept. 2014.
- [15] M. Gapeyenko, A. Samuylov, M. Gerasimenko, D. Moltchanov, S. Singh, E. Aryafar, S. Yeh, N. Himayat, S. Andreev, and Y. Koucheryavy, "Analysis of human-body blockage in urban millimeter-wave cellular communications," in *Proc. of the IEEE International Conference on Communications (ICC)*, May 2016, pp. 1–7.
- [16] E. Hriba, M. C. Valenti, K. Venugopal, and R. W. Heath Jr., "Accurately accounting for random blockage in device-to-device mmwave networks," in *Proc. of the IEEE Global Communications Conference (GLOBECOM)*, Dec 2017, pp. 1–6. [Online]. Available: <https://arxiv.org/abs/1709.00521>
- [17] M. Dong and T. Kim, "Reliability of an urban millimeter wave communication link with first-order reflections," in *Proc. of the IEEE Global Communications Conference (GLOBECOM)*, Dec 2016, pp. 1–6.
- [18] A. Samuylov, M. Gapeyenko, D. Moltchanov, M. Gerasimenko, S. Singh, N. Himayat, S. Andreev, and Y. Koucheryavy, "Characterizing spatial correlation of blockage statistics in urban mm-wave systems," in *Proc. of IEEE Globecom Workshops*, Dec 2016, pp. 1–7.
- [19] F. Baccelli and X. Zhang, "A correlated shadowing model for urban wireless networks," in *IEEE Intl. Conf. on Computer Communications (INFOCOM)*, Hong Kong, April 2015, pp. 801–809.
- [20] S. Aditya, H. S. Dhillon, A. F. Molisch, and H. Behairy, "Asymptotic blind-spot analysis of localization networks under correlated blocking using a poisson line process," *IEEE Wireless Commun. Lett.*, vol. 6, no. 5, pp. 654–657, Oct. 2017.
- [21] D. Stoyan, S. N. Chiu, W. S. Kendall, and J. Mecke, *Stochastic geometry and its applications*, 3rd ed. Wiley, 2013.
- [22] S. Boyd and L. Vandenberghe, *Convex Optimization*. New York, NY, USA: Cambridge University Press, 2004.
- [23] D. Stoyan, S. N. Chiu, W. S. Kendall, and J. Mecke, *Stochastic geometry and its applications*, 3rd ed. Wiley, 2013.
- [24] A. Papoulis, S. Pillai, and S. Unnikrishna, *Probability, random variables, and stochastic processes*. McGraw-Hill New York, 2002, vol. 73660116.